Application of Solidification Theory to Rapid Solidification Processing

W. J. Boettinger, J. W. Cahn, S. R. Coriell,
J. R. Manning, and R. J. Schaefer
Metallurgy Division
Center for Materials Science
National Bureau of Standards
Washington, DC 20234

Semi-Annual Technical Report
Period Covered: October 1, 1982 to March 31, 1983

Report Issued: August 1983

Prepared for
Defense Advanced Research Projects Agency
Arlington, Virginia 22209

AO 3751

Program Code No: 9D10
Effective Date of Contract: April 1, 1979
Contract Expiration Date: March 31, 1984
Principal Investigator: J. R. Manning (301/921-3354)

Table of Contents

Application of Solidification Theory to Rapid Solidification Processing

1. Technical Report Summary

This semi-annual technical report for ARPA Order 3751 covers the period October 1, 1982 to March 31, 1983. Significant accomplishments during that period were achieved in the following areas:

Microstructures Obtained in Rapidly Solidified Alloys

- Related critical velocity for production of microsegregation free Ag-Cu alloys in the extended solid solubility range to kinetic limits on solute trapping and to thermodynamic limits arising from the T_o curve.
- Determined upper and lower bounds on solidification velocity which produce a special "banded" microstructure in Ag-Cu alloys. Related lower bound to theoretical limits on solidification velocity for eutectic and cellular microstructures.
- Measured microstructures produced in rapidly solidified NiAl-Cr alloys. Found partitionless columnar grains with fine rod-like eutectic structures between grains.
- Determined that ordered NiAl-type structure was initially produced during partitionless rapid solidification of NiAl-Cr quasibinary eutectic alloy rather than a disordered structure incorporating Ni and Al into Cr randomly. Related this result to T_o curves in NiAl-Cr.

Segregation-Free Solidification in Rapidly Solidified Alloys

- Calculated temperature-composition response curve as a function of solidification velocity for Ag-Cu alloys. Such curves are important in considering recalescence phenomena and interface stability during solute trapping.

- o Demonstrated effect of temperature-dependence of liquid diffusion coefficients on rapid solidification and production of microsegregation-free alloys.
- o Determined restrictions on application of absolute stability theory to segregation-free solidification. Range of applicability includes successful predictions for Ag-Cu alloys.

Precipitation Processes in Rapidly Solidified Alloys

- o Demonstrated a significant effect of the microstructures formed during rapid solidification on precipitation processes in Al-Mn alloys.
- o Correlated the presence of a cellular substructure in rapidly solidified Al-Mn alloys to an incomplete incorporation of Mn into the Al lattice.
- o Demonstrated that the stability of the supersaturated solid solution of Mn in Al at 450°C is strongly affected by the location of Al_6Mn precipitates and that the sites of the Al_6Mn precipitates are strongly sensitive to the rapid solidification microstructure.
- o Demonstrated that the G phase ($Al_{12}Mn$), when present, increases in abundance at long annealing times, but that the growth rate of this phase is strongly affected by the microstructure-dependent distribution of Al_6Mn.

Task Objective

The objective of this work is to develop guidelines based on kinetic and thermodynamic solidification theory for prediction and control of rapid solidification processes. In particular, segregation effects and rules governing the formation of equilibrium and non-equilibrium phases, will be investigated. Areas where significant improvements in alloy properties can be produced by rapid solidification will be emphasized.

Technical Problem and General Methodology

Rapid solidification techniques make it possible to produce new types of materials having significantly better properties than conventionally processed materials. However, improved predictive techniques and control of rapid solidification processes are needed. The current studies are focussed on the science underlying areas where improved materials can be obtained in order to provide such prediction and control. This work is both theoretical and experimental.

Ways in which rapid solidification produces special properties in alloys include:

A. Extended solid solubility
   - provides alloys with high solute content, not normally available to design engineers.

B. Enhanced homogeneity, improved microstructures
   - creates more uniform alloys and allows formation of fine precipitates with resulting improvements in mechanical properties.

C. Formation of new alloy phases not normally obtainable
   - produces entirely new types of materials, including new crystalline phases as well as metallic glass alloys

D. Alloy surface modification by rapid melting-and-refreezing
   - modifies the alloy surface, for example, to provide protective coatings without altering bulk properties of the substrate

Significant accomplishments have been achieved during the course of this contract in each of these areas.

Critical solidification velocities needed for formation of metallic glass in Pd-Cu-Si alloys were measured in work completed earlier in this contract. These results apply directly to application area C above and also bear on current work on extended solubility (area A above). A theory with broad applicability to many alloy systems, as well as to production of extended solubility alloys, was developed to explain the measured results. It was shown that at alloy compositions where the T_o curve

on the phase diagram plunges to very low temperatures, crystallization is feasible only by separation of alloy constituents into two phases. The resultant need for diffusional separation of alloy constituents produces a maximum limit on crystal solidification velocity. At velocities above this limit, which typically would be the order of 5 cm/s, amorphous alloys will be produced in place of crystalline alloys. This work showed the importance of the limits on eutectic solidification velocities. Crystal nucleation rates clearly were not the limiting factor in production of the amorphous Pd-Cu-Si in these experiments since the alloy consistently was observed to change from crystalline eutectic solidification to amorphous solidification as the growth rate in an alloy ribbon was accelerated through the critical velocity. These measurements and the accompanying predictions of critical solidification velocities provide guidelines for processing and control of the properties of such alloys.

Many of these same principles concerning T_o (thermodynamic) and diffusion rate (kinetic) restrictions on production of amorphous alloys can also be applied to production of homogeneous metastable <u>crystalline</u> alloys. The main difference is that to produce amorphous alloys the T_o curve should lie well below the liquidus so that the glassy structure is frozen in place before temperature T_o is reached whereas to produce homogeneous crystalline alloys in the metastable extended-solubility composition range, it must be possible to undercool to a temperature below T_o while still being at a sufficiently high temperature to allow crystallization kinetically to occur.

As examples of significant results concerning alloy surface processing in application area D, measurements have been made of the tendency of cracks to appear in surface melted-and-refrozen layers due to the stresses introduced by rapid solidification and of conditions necessary to produce convective mixing in rapidly solidified surface layers. The rapidly solidified layers in these experiments were produced by scanning an electron beam across an alloy

surface. Conclusions on these topics were presented, respectively, in the semi-annual reports covering work on this contract for October 1981-March 1982 and April 1982-September 1982. The cracking problem often is serious enough so that it would prevent practical use of rapidly solidified surface layers and coatings. Convective mixing is important to produce homogeneity in these surface layers and coatings. The current results provide at least some initial insight to guide practical applications in these areas.

Most recently, the work on this contract has centered on studies of the special microstructures, segregation effects, precipitation processes and extended solid solubility found in rapidly solidified alloys (areas A and B above). It is found, for example, that production of alloys with extended solid solubility under suitable conditions will result in micro-segregation-free crystalline alloys. Heat treatment of these alloys then may lead to production of large volume fractions of fine precipitates with resulting improvements in mechanical properties, and even to the appearance of precipitate phases not obtainable by other means. These processes and effects are being investigated as described in the following section. Theories which are being developed to explain these results will provide guidelines for control of these processes and for the tailoring of compositions and processing conditions to obtain desirable alloy properties.

Technical Results; Important Findings and Conclusions; Implications for Future Work

A major feature of rapid solidification processing (RSP) is the possibility of producing segregation-free alloys. These homogeneous alloys because of their absence of compositional variation will have more uniform properties than conventionally produced alloys, thus providing greater reliability and uniformity of performance. Micro-segregation-free RSP alloys can be produced both in the equilibrium solubility range and in the extended solubility composition range.

Precipitation processes are important for rapidly solidified alloys which achieve extended solid solubility. Such metastable alloys upon heat treatment or thermomechanical processing can be expected to transform into more stable states, for example forming two-phase microstructures not obtainable by other means. Experimental and theoretical investigations during the current reporting period have produced a number of results pertinent to micro-segregation-free alloys, extended solubility in RSP alloys and precipitation processes in such alloys. These results comprise the bulk of the present report.

These results include (a) a systematic study of the microstructures formed in Ag-Cu alloys with compositions from 1 wt% Cu (in the equilibrium solid solubility range) to 28.1 wt% Cu (the eutectic composition) and solidification velocities from 1.5 cm/s to 400 cm/s, (b) development of theories on the mechanism of segregation-free solidification, applicable both to Ag-Cu and to a wide range of other alloys, (c) studies of precipitation processes in Al-Mn RSP alloys having compositions in the extended solid solubility range (up to 12 wt% Mn), (d) measurements of microstructures formed by rapid solidification of NiAl-Cr quasibinary eutectic alloys, where NiAl has an ordered bcc structure and the Cr-rich phase has a disordered bcc structure.

Results in each of these four areas were presented in papers at the Third Conference on Rapid Solidification Processing; Principles and Technologies, held at the National Bureau of Standards, Gaithersburg, Maryland, December 6-8, 1982. These papers are included in an appendix as part of this report and also will appear on the published conference proceedings. Important findings, conclusions and implications for future work are discussed in some detail in these papers, and they provide the bulk of the technical results pertinent to this report. For purposes of emphasis, however, some of the more significant of these results will now be highlighted in the following sections.

(a) Systematic Measurement of Microstructures Obtained in Rapidly Solidified Ag-Cu Alloys

Silver-copper alloys were investigated as a model system to test effects of rapid solidification in producing extended solid solubility. The two terminal phases in this alloy system both have fcc structures and the phase diagram shows a simple eutectic between these terminal phases with the eutectic composition being 28.1 wt% Cu. The equilibrium solubility limit for Cu in Ag is about 8 wt% Cu. Phase diagram calculations in the metastable range above 8 wt.% Cu indicate that the T_o curve in the composition range up to the eutectic composition lies less than a hundred degrees below the liquidus so that undercooling below the T_o temperature should be readily obtainable during rapid solidification. These features all make Ag-Cu a good system for application of predictive modeling.

Electron beam surface melting and resolidification passes were performed on Ag-Cu alloys containing approximately the following weight per cents of copper: 1, 5, 9, 15, 23 and 28.1. At all compositions, it was found possible to produce homogeneous single phase alloys having the average composition of the melt. In other words, extended solid solubility (above 8 wt% Cu) was produced all the way up to the eutectic composition. This result is consistent with the guideline previously postulated in this work that extended solid solubility is possible if the melt can be undercooled below the T_o temperature. Here, T_o is the temperature at which the liquid and crystalline solid of the same composition have the same free energy. This temperature varies with composition and its locus can be plotted as a curve on the phase diagram.

Even though it is thermodynamically possible according to the phase diagram, extended solid solubility will not occur unless the kinetic conditions cause it to be produced. Thus, kinetic measurements were made at each composition by varying the scan velocities of the electron beam,

with the solidification velocity depending on the scan velocity, to determine the critical scan speed required to produce microsegregation-free alloys.

In the 1% and 5% alloys which were within the equilibrium solid solubilit range, a single phase alloy normally would be expected to be produced. Thus, steady state solidification at a planar interface should produce a homogeneous single-phase alloy at these compositions. Such alloys were found with the critical solidification velocity for transition from cellular to planar solidification increasing with composition. The critical velocity increased from about 20 cm/s in the 1% alloy to about 60 cm/s in the 5% alloy. This is consistent with morphological stability predictions made in earlier work on this contract.

In the extended solid solubility range, the alloy normally should solidif in a two-phase cellular, dendritic or lamellar structure with diffusional sort of atom species occurring during the solidification. However, a homogeneous a will result if the solidification front advances rapidly enough to trap the solute in place before diffusional sorting or motion of a rejected species away from an advancing dendrite tip can occur in the liquid. Thus, one has not only the thermodynamic requirement that the undercooling be sufficient to effectively reduce the melt temperature below T_o but also the kinetic requirement that the solidification velocity be above a certain speed, measured in Ag-Cu to range from about 200 cm/s for 15 wt% Cu alloys down to about 70 cm/s at the eutectic composition. Understanding this interpl of thermodynamic and kinetic limits will be important in providing prediction and control of these processes.

An additional phenomenon that occurs in the Ag-Cu alloys in the extended solid solubility composition range is the appearance of banded microstructures the solidification velocity has an intermediate value. Alternating bands were formed parallel to successive solidification interface positions with micro-segregation-free material appearing in one band, cellular microstructures in t

next alternate band, then microsegregation free material in the next band, and so on. The lower velocity bound for this special banded microstructure may correspond to the maximum growth rate of dendritic and eutectic growth in concentrated alloys and the upper velocity bound to the rate needed to cause sufficient deviation from interfacial equilibrium to increase the partition coefficient to unity and thus allow full partitionless solidification.

This work is reported in more detail in a paper by W. J. Boettinger, R. J. Schaefer, F. Biancaniello, and D. Shechtman, entitled "The Effect of Solidification Velocity on the Microstructure of Ag-Cu Alloys." This paper is included as an appendix in this report and will be published in the Proceedings of the Third Conference on Rapid Solidification Processing: Principles and Technologies. As part of a cooperative arrangement, the electron microscopy of these alloys was performed by D. Shechtman of the Johns Hopkins University, Center for Materials Science during time spent at NBS.

(b) Mechanisms of Segregation-Free Solidification

Two solidification mechanisms can produce microsegregation-free crystalline solids: planar growth and partitionless solidification. In a paper by W. J. Boettinger, S. R. Coriell and R. F. Sekerka entitled "Mechanisms of Segregation-Free Solidification," topics related to the solidification conditions required to produce such microstructures are described. This paper included as an appendix in this report and will be published in the Proceedings of the Third Conference on Rapid Solidification Processing: Principles and Technologies. R. F. Sekerka, who is a co-author of this paper, is with Carnegie-Mellon University and serves as consultant to NBS on this RSP program and other programs.

Three major topics are discussed in this paper: (1) the interface temperature during solute trapping, (2) factors influencing microsegregation-free solidification in concentrated alloys, and (3) conditions under which absolute stability theory is valid.

The relation of solute trapping and interface temperature to solidification velocity can be visualized in terms of a response curve drawn on the phase diagram. At zero solidification velocity, the composition of the solid that is formed lies on the solidus curve in the phase diagram with the temperature of the solidification interface equalling that of the liquid. At intermediate solidification velocities, the concentration of the solid moves toward that of the liquid with a small amount of undercooling being produced. At very rapid solidification velocities in an alloy such as Ag-Cu where partitionless solidification is possible, the undercooling greatly increases and the composition of the solid approaches that of the liquid as a result of solute trapping. This temperature-composition response curve was calculated for Ag-Cu. Such curves are required for a detailed analysis of interface stability during solute trapping and of recalescence phenomena where the velocity of the interface starts out at a high value and then decreases because of the evolution of latent heat.

The experimental results on Ag-Cu show a clear dependence on composition of the critical velocity for production of microsegregation-free crystalline alloys, the required velocity noticeably decreasing in the range 15 to 28 wt% Cu. Simple solute trapping models, however, include no composition dependence. It is noted that one possible cause of the observed composition-dependence is the dependence of liquid diffusion coefficients on temperature. This effect could become important as a result of changes in the amount of undercooling required to reach the T_0 curve as composition is varied, since the diffusion coefficient depends on temperature.

Absolute stability theory was successful in predicting critical solidification velocities for production of microsegregation-free Ag-Cu alloys within the equilibrium solid solubility range (less than 8 wt% Cu). The range of applicability of this theory was investigated to determine how broadly these principles can be applied. One significant restriction is the requirement that the

heat flow, including that arising from latent heat released during solidification, be directed primarily into the solid rather than the liquid.

(c) Precipitation in Rapidly Solidified Al-Mn Alloys

Supersaturated Al-Mn alloys were prepared by melt-spinning. These were characterized both before and after subsequent annealing at 450° C in order to evaluate precipitation processes in these rapidly solidified alloys. Some of these results are reported in a paper by R. J. Schaefer, M. Rosen, J. J. Smith, D. Shechtman and R. Mehrabian entitled "Nondestructive Characterization of Rapidly Solidified Al-Mn Alloys." This paper is included as part of this report in the appendix and will be published in the Proceedings of the Third Conference on Rapid Solidification Processing; Principles and Technologies. The co-authors M. Rosen, J. J. Smith and D. Shechtman are with Johns Hopkins University. They collaborated in this work at NBS as part of a cooperative program with NBS scientists on characterization and non-destructive evaluation.

It was found that there was a significant influence of rapid solidification on precipitation processes in these alloys. For example, new phases not formed during conventional processing were produced. These differences in precipitation behavior presumably arise because the microstructure and state of supersaturation of the alloy are significantly different after rapid solidification from those obtained after conventional processing.

Annealing of these alloys at 450° C results in precipitation of two phases; Al_6Mn and "G" phase, the latter having the composition $Al_{12}Mn$. Al_6Mn is known to be the stable phase at temperature above 500° C but the relative stability of the two phases at lower temperatures is not clear. In all of the rapidly solidified alloys the amount of G phase increased relative to the Al_6Mn phase at long annealing times, thus implying that the former is the stable phase

at 450° C. Our experiments have shown that the relative abundance of the two precipitating phases at different stages of annealing is determined by the microstructures developed during the rapid solidification process. The different nucleation sites and growth kinetics of the two precipitating phases combine to yield their result.

(d) Microstructures Formed by Rapid Solidification of NiAl-Cr Quasibinary Eutectic Alloys

Rapidly solidified ribbons of NiAl-Cr quasibinary eutectic composition were produced by melt-spinning. Here Cr is regarded as one component and NiAl as the second component in this quasibinary. Although solidification velocities from this process are not known, much of the rapidly quenched alloy was observed to consist of columnar grains having the composition of the melt, indicating that at least a moderate amount of undercooling had been achieved.

The volume between these grains showed a fine rod-like eutectic structure. It is presumed that the columnar grains solidified by partitionless solidification in regions where the solidification velocity was too fast to allow separation into the two-phase eutectic structure. Between grains where the solidification proceeded more slowly, perhaps slowed down by the release of latent heat of fusion, separation into Cr-rich and NiAl-rich phases could occur. Eutectic spacings as small as 12 nm were measured.

These solidification processes are of particular interest because the NiAl and Cr phases are crystallographically very similar, NiAl exhibiting an ordered structure (CsCl) which has the same underlying bcc arrangement as does the disordered Cr phase in this quasibinary. Moreover, the lattice mismatch between these two phases is small. This is consistent with having the T_0 curve lying near the liquidus so that only a moderate

amount of undercooling would be required to allow partitionless solidification to occur. An intriguing aspect of the columnar alloy is that it appears to have solidified with the ordered NiAl structure rather than in the simpler disordered Cr structure. A thermodynamic explanation for this effect, which may have implications for rapid solidification of other ordered alloys, can be provided by noting that the T_0 curve for the ordered phase very likely is located at a higher temperature in the eutectic composition region than is the T_0 curve for the disordered alloy. Consequently less undercooli is required to produce the ordered partitionless alloy than the disordered phase.

These results are reported in a paper by D. Shechtman, T. Z. Kattamis, F. S. Biancaniello and W. J. Boettinger entitled "The Microstructure of Rapidly Solidified NiAl-Cr Quasibinary Eutectic." This paper which will appear in the Proceedings of the Third Conference on Rapid Solidification Processing: Principles and Technologies is included as part of this report in the appendix. D. Shechtman of the Johns Hopkins University, Center for Materials Science, and T. Z. Kattamis of the University of Connecticut, Department of Metallurgy, collaborated in this work with NBS scientists during time spent at NBS.

roceedings of Rapid Solidification Processing: Principles and Technologies (III) edited by . Mehrabian, NBS Internal Report (1983)

MECHANISMS OF SEGREGATION-FREE SOLIDIFICATION

W. J. Boettinger, S. R. Coriell

Metallurgy Division
National Bureau of Standards
Washington, DC 20234

and

R. F. Sekerka*

Carnegie-Mellon University
Pittsburgh, PA 15213

ABSTRACT

A frequent microstructural feature of rapidly solidified alloys is the absence of cellular or dendritic microsegregation, often accompanied by incorporation of solute in excess of the equilibrium solid solubility. Two solidification mechanisms can produce microsegregation-free crystalline solids: planar growth and partitionless solidification. The solidification conditions required for planar growth with equilibrium partitioning at the interface are well known. For growth at high velocities, capillarity provides a stabilization of the planar interface. This regime is referred to as absolute stability and applies only when the net heat flow is toward the solid. Partitionless solidification arises from the kinetics of interface motion. These kinetics can involve the trapping of solute by the moving interface, causing the partition coefficient to deviate from the equilibrium value. Solute trapping generally occurs at high interface velocities and may be pronounced when the interface temperature is far below the liquidus. In the limit of partitionless solidification, when the partition coefficient is unity, the interface temperature is below the T_0 temperature for the composition at the interface. Partitionless solidification provides a mechanism for the formation of segregation-free crystalline alloys when the net heat flow is toward the liquid or when the interface is not planar. Recent work has combined a velocity dependent partition coefficient with interface stability theory to predict the solidification conditions required for microsegregation-free solidification. Under some conditions, oscillatory instabilities are predicted. The relation of the interface temperature to the liquidus, solidus and T_0 temperatures as a function of growth rate and considerations necessary to predict the conditions of microsegregation-free solidification in concentrated alloys are discussed.

Introduction

Microsegregation-free crystalline alloys including those with solute in excess of equilibrium solubility provide an ideal starting microstructure for the development of interesting mechanical properties during subsequent thermomechanical processing [1]. In this paper, the following three topics related to the solidification conditions required to produce such microstructures will be described: the interface temperature during solute trapping; the interface stability theory; and the conditions for microsegregation-free solidification of concentrated alloys. It will be assumed that the phase which is forming from the melt has been selected previously by nucleation kinetics or by competition among growing crystalline phases. Under this assumption, the primary role of nucleation is to allow the development of a large bulk undercooling of the liquid into which growth can occur quite rapidly. This paper focuses on the conditions at the solid-liquid interface, with the realization that a full analysis of heat and solute transport must be conducted to form the basis for a final choice of processing conditions.

*Consultant, National Bureau of Standards

Interface Conditions

In 1971, Baker and Cahn [2] posed the solidification problem of a binary alloy using two response functions. One choice for the response functions describes the interface temperature, T_I, and the composition of the solid at the interface, C_s^*. These response functions can be written as follows:

$$T_I = f(V, C_L^*) - T_M \Gamma K \tag{1}$$

$$C_s^* = C_L^* k(V, C_L^*) \tag{2}$$

where V is the local interface velocity, C_L^* is the composition of the liquid at the interface, $T_M\Gamma$ is a capillarity constant, and K is the mean curvature of the solid-liquid interface. At zero velocity, the functions f and k are very simply related to the phase diagram: $f(0,C_L^*)$ is the equation for the phase diagram liquidus and $k(0,C_L^*)$ is the equation for the equilibrium partition coefficient, k_E, which can depend on composition.

These response functions are constrained by thermodynamics. Fig. 1 shows the molar free energy versus composition for a liquid and a solid phase at a fixed temperature. During solidification, the temperature and the compositions at the interface are constrained by the fact that there must be a net decrease in the free energy per mole, ΔG_f needed to form an infinitesimal amount of solid of composition C_s^* from liquid of composition C_L^* [2]. The free energy change is shown in Fig. 1, and is given by

$$\Delta G = (\mu_s^A - \mu_L^A)(1 - C_s^*) + (\mu_s^B - \mu_L^B)C_s^*. \tag{3}$$

Under the usual assumption of local equilibrium at the solid-liquid interface, believed to be valid at slow rates of solidification, the chemical potentials of the liquid, μ_L^i, and solid, μ_s^i, for each species, i, must be equal. During rapid rates of solidification, this is not necessarily the case and nonequilibrium conditions at the interface can exist. The term solute trapping is loosely applied to conditions when the partition coefficient deviates from the equilibrium value, but as originally defined, is restricted to the case when the chemical potential of the solute increases during solidification. Baker and Cahn showed that the restriction that ΔG be negative could be represented on a figure where, for constant temperature, the range of possible solid and liquid

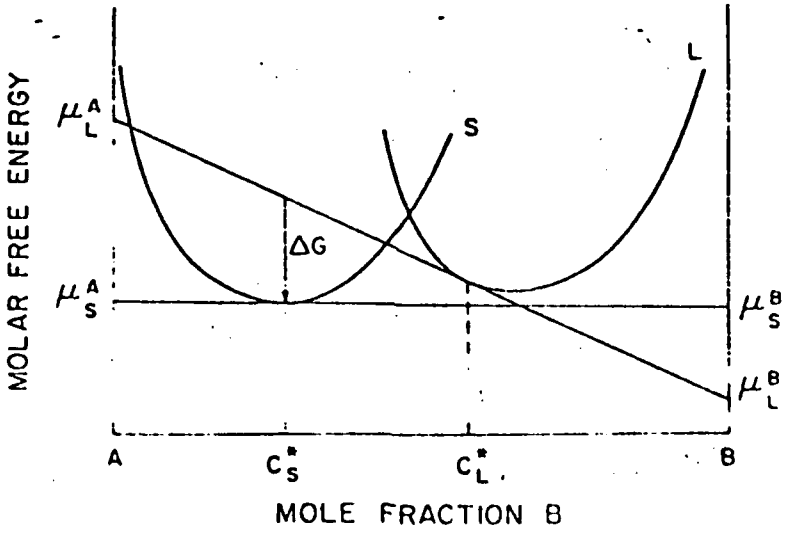

Fig. 1. Construction to show the Gibbs free energy per mole, ΔG, for solidification of an infinitesimal amount of solid of composition C_s^* from a liquid of composition C_L^* under nonequilibrium conditions for which the chemical potentials $\mu_L^A \neq \mu_s^A$ and $\mu_L^B \neq \mu_s^B$.

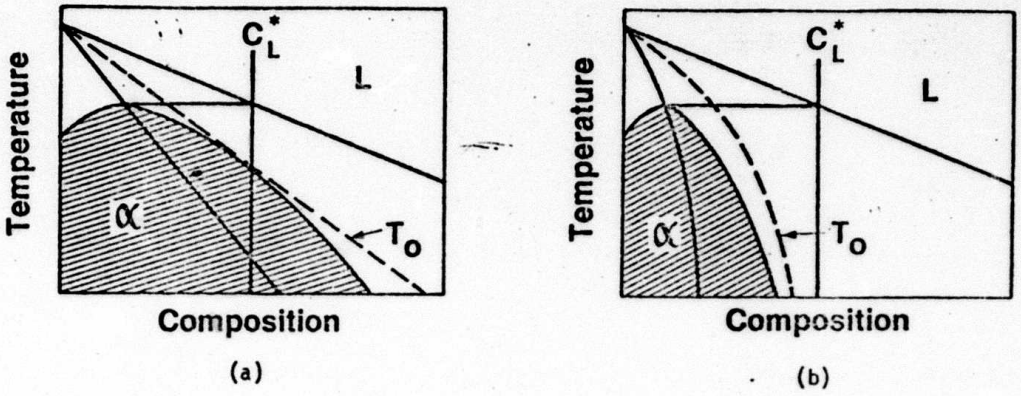

Fig. 2. Regions (cross-hatched) of thermodynamically allowed solid compositions that may be formed when solid solidifies from liquid of composition C_L^* at various temperatures. The value of T_o is the highest temperature at which partitionless solidification of a liquid of given composition can occur. In (b), the T_o curve plunges and partitionless soldification is impossible for liquid of composition C_L^*. (From reference [3]).

concentrations are shown. Fig. 2 shows an alternate representation of this restriction [3]. The cross-hatched region shows the range of possible solid compositions that can form from a liquid of composition C_L^* at various temperatures. When the temperature is equal to the liquidus temperature for the composition C_L^*, the only possible solid composition is the equilibrium solid composition. For interface temperatures below the liquidus, the range of allowable solid composition expands. Of particular interest is the T_o curve which lies between the liquidus and and solidus. The T_o curve is the locus of compositions and temperatures for which the molar free energy of the liquid and solid phases are equal. When the temperature of the liquid at the interface reaches the T_o curve, the solid can have the same composition as the liquid, i.e., partitionless solidification. Fig. 2b shows a case where the T_o curve plunges quite steeply. In this case, for the composition C_L^*, partitionless solidification is not possible, i.e., the partition coefficient, k, cannot approach unity at high velocity.

Many models for the dependence of the partition coefficient on velocity have been formulated [4-7]. This dependence on velocity constitutes one of the two response functions required to analyze rapid solidification problems. The model formulated by Baker [4] is quite general and includes a wide variety of possibilities. Fig. 3 shows the results of more recent theories which predict that the partition coefficient changes monotonically from its equilibrium value to unity as the growth velocity increases. In these models the interface partition coefficient is a function of a dimensionless velocity, $\beta_o V$, where β_o is the ratio of a length scale, a_o, normally related to the interatomic distance and a diffusion coefficient, D. The diffusion coefficient in the various models ranges between a liquid diffusion coefficient and a diffusion coefficient characteristic of the interface itself. The functional form of the model proposed by Aziz [5] and Jackson, Gilmer and Leamy [6] for continuous growth is given as

$$k(V) = \frac{k_E + \beta_o V}{1 + \beta_o V} \qquad (4)$$

where $\beta_o = a_o/D$. At a velocity of $1/\beta_o$, the partition coefficient is the average of the equilibrium partition coefficient and unity. If we choose a liquid diffusion coefficient typical of metals (10^{-5} cm^2/s) and the length scale to be 5Å, $1/\beta_o$ is 200 cm/s. However, the value of $1/\beta_o$ which best fits [5] recent experimental data for doped Si is 10 m/s; for Si, D = 5 x 10^{-4} cm^2/s [8], and hence a_o = 50 Å. It remains a challenge to design good experiments to determine the velocity required for solute trapping in metallic alloys.

There are significant shortcomings in the present models of the dependence of the partition coefficient on velocity. The models primarily treat dilute alloys so there is no explicit dependence on composition. For the case of Fig. 2b, where the T_o curve plunges, the partition coefficient cannot approach unity at high velocity. A second shortcoming of the present trapping models is that the response function for the interface temperature is not treated.

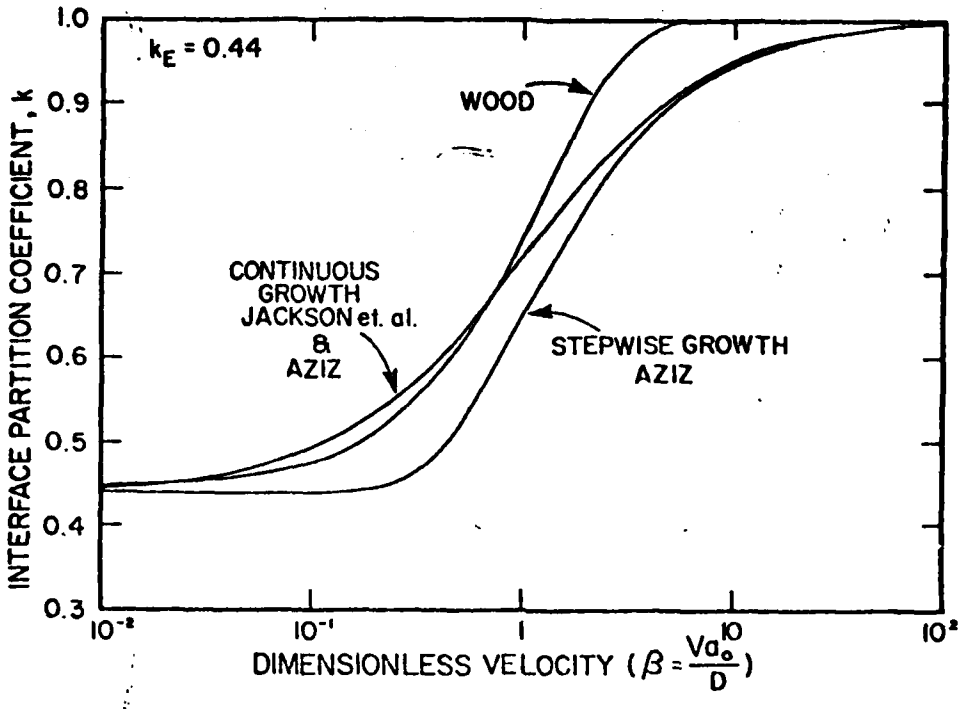

Fig. 3. Curves showing the dependence of the interface partition coefficient, k, on velocity according to the models of various investigators.

Following the suggestion of Aziz [5] a model for the response function for the interface temperature can be formulated. For pure materials Turnbull et al. [9,10] have suggested that the rate at which atoms attach to the growing crystalline solid may only be limited by their rate of collision with the solid. In such a case, the interface velocity is related to the interface temperature, T_I, by an expression

$$V = fV_o\{1-\exp(\Delta G/RT_I)\} \tag{5}$$

where f is the fraction of sites on the solid-liquid interface available for attachment, V_o is the speed of sound in the liquid metal, ΔG is the molar free energy for solidification and R is the gas constant. For most metals, f is thought to be close to unity and for velocities much less than the speed of sound, this expression can be written as

$$V = -V_o\left(\frac{\Delta G}{RT_I}\right). \tag{6}$$

For the solidification of disordered crystals, this collision limited model of solidification may apply as well. This model will be employed to formulate a response function for the interface temperature for a binary alloy. The molar free energy for solidification is evaluated from Eq. (3) and, in special cases, can be described simply in terms of undercooling. When solute trapping occurs a simple expression in terms of undercooling is not possible. For pure metals ΔG reduces to

$$\Delta G = \frac{-L(T_M-T_I)}{T_I} \tag{7}$$

where L is a latent heat and T_M is the melting point of the pure metal. For dilute alloys, when the partition coefficient equals the equilibrium partition coefficient, k_E, the thermodynamic driving force for solidification is given by

$$\Delta G = \frac{-L(T_L - T_I)}{T_I} \qquad (8)$$

where T_L is the liquidus temperature for the concentration of the liquid at the interface C_L^*. When the partition coefficient is identically equal to one, ΔG has a similar form,

$$\Delta G = \frac{-L'(T_o - T_I)}{T_I} \qquad (9)$$

where L' is a composition weighted latent heat, and the T_0 temperature corresponds to the interface composition. The similarity of the expressions for the case where k equals one, i.e., partitionless solidification, and the expression for pure metals, is the origin of the often stated idea that the kinetics of partitionless solidification are quite rapid and similar to that for the solidification of a pure metal. In the general case when the partition coefficient is not the equilibrium value, the thermodynamic driving force for solidification must be evaluated from the full expression given by Eq. (3). In this expression the chemical potentials are functions of concentration and temperature that may be determined by modelling the phase diagram. This demonstrates the importance of modelling phase diagrams, even for applications to rapid solidification. If Eqs. (3 & 5) are combined with, for example, the trapping model of Aziz, Eq. (4), the interface temperature can be determined as a function of the interface velocity and the concentration of the liquid at the interface. A similar calculation for other models of solute trapping or interface temperature can be performed. Alternatively, part of the free energy for solidification can be dissipated by solute drag, as reported by Aziz in the current proceedings [11].

Fig. 4 shows a composite plot of the two response functions obtained by using Eqs. (3-5) superimposed on the phase diagram including the liquidus, solidus and T_0 curve. The composition of the solid at the interface and the interface temperature are plotted along a curve parameterized by interface velocity for a given fixed liquid concentration at the interface. The figure is based on thermodynamic data for Ag-Cu [12], a liquid composition of 8.2 at% Cu, a value of β_o of 10^{-2} s/cm and for two values of V_o (infinity and 2×10^5 cm/s). At zero velocity, the composition of the solid lies on the solidus curve. At intermediate velocities (~10 cm/s), the concentration of the solid moves towards the concentration of the liquid with a small increase in the undercooling. At high velocities the solid composition at the interface approaches the liquid concentration at the interface near the T_0 curve. The dashed curve shows the case where V_0 is infinite. This corresponds to the thermodynamic bound on the solid concentration at the interface given in the Fig. 2. The dashed curve can also be obtained by letting $\Delta G = 0$ in Eq. (3). The solid curve, for a finite value of V_0, shows the interface temperature plunging quite rapidly. This analysis provides, for the first time, a pair of response functions for the conditions at the liquid-solid interface, thus permitting the analysis of rapid solidification problems when combined with solute redistribution and heat flow analysis. Such curves are of interest during recalescence when the velocity of the interface starts out at a high value and decreases due to the evolution of latent heat. They are also required for a detailed analysis of the stability of the solid-liquid interface during solute trapping.

Interface Stability

Interface stability theory is of interest because, during planar growth, solidification occurs with no lateral microsegregation. The theory was first developed by Mullins and Sekerka [13] and has been extended and discussed in more detail for rapid solidification by Coriell and Sekerka [14-15]. The present paper is restricted to a discussion of the simple asymptotic form of the stability theory relevant at high velocity. This asymptotic form is known as absolute stability and is given by the expression

$$V = \frac{mD(1-k_E)C}{k_E^2 T_M \Gamma} \qquad (10)$$

where m is the liquidus slope, D is the liquid diffusion coefficient and C is the alloy composition. Whenever V exceeds the value given in Eq. (10), a planar liquid-solid interface is stable. Absolute stability of a planar interface occurs because of the influence of capillarity. At high growth velocities, there is only limited time available so lateral solute segregation in the liquid can

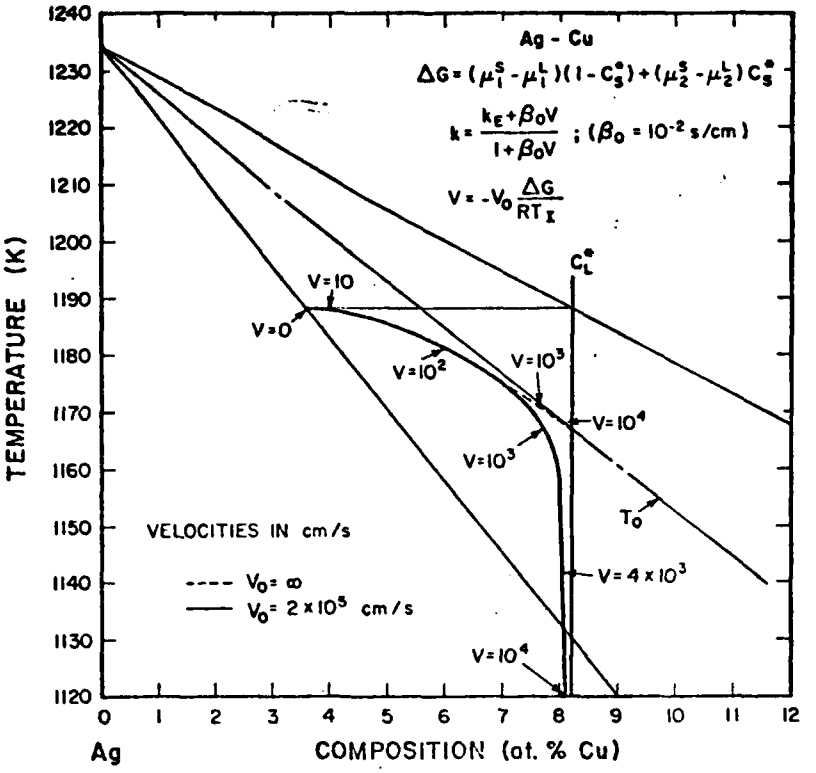

Fig. 4. Interface temperature and solid compositions for solid that forms at the indicated velocities from a liquid of fixed composition C_L^* at the interface. Thermodynamic parameters are for Cu in Ag for a specific kinetic law with $V_0 = 2 \times 10^5$ cm/s (full curve) and $V_0 \to \infty$ (dashed curve).

only occur for perturbations of the solid-liquid interface with very short wavelengths. These short wavelengths require such a large increase in the area of the interface that the perturbations are retarded by capillary forces and the interface is stable.

There are several restrictions on the use of the simple asymptotic form given by Eq. (10). First, rather trivially, this form is only valid if the partition coefficient is the equilibrium partition coefficient. Modifications required when the partition coefficient depends on the velocity will be discussed in a later section. A second restriction is that the net heat flow must be into the solid, i.e.,

$$G^* = \frac{k_L G_L + k_S G_S}{k_L + k_S} > 0. \qquad (11)$$

Here k_L and k_S are the thermal conductivities of the liquid and solid respectively. G_L and G_S are the temperature gradients in the liquid and solid respectively. In the case of solidification following surface melting, the conduction of heat is almost completely into the solid and G^* is always positive. For quenching against a substrate or for atomization, the sign of G^* is less clear. What is important is the relative amount of heat flowing into the solid and flowing into the liquid. For quenching against a substrate, bulk undercooling of the liquid can occur if nucleation is difficult. In this case, during solidification heat can flow both into the solid and into the liquid to remove the latent heat evolved at the liquid-solid interface. An experimental observation in which planar growth is stable, and G^* is negative, would require a reexamination of the assumptions

in the present stability theory. In this event two possible modifications [14] would be an allowance for a velocity of solidification that depends on time or an analysis of solidification in samples in which the wavelength of the fastest growing instability is of the same order as the sample itself. A third restriction on the use of the absolute stability equation is that one must be far from the modified constitutional supercooling regime of the full stability theory. This condition will be satisfied whenever the velocity

$$V >> \frac{LD^2}{(k_s+k_L)T_M\Gamma k_E}, \tag{12}$$

provided also that the temperature gradient in the liquid is not too large [$G_L << VL/(2k_L)$] as is usually the case for rapid solidification. Here, L is the latent heat per unit volume. This restriction is more important for doped Si [15] than for metallic alloys due to the relatively high latent heat and diffusion coefficient for Si.

In a recent set of experiments employing electron beam surface melting [16-17] the applicability of the morphological stability theory to rapid solidification has been demonstrated. Fig. (5) shows the transition from cellular to cell-free structure which occurs in Ag-1 wt% Cu and Ag-5 wt% Cu alloys. For the former, the transition occurs between 10 and 20 cm/s, and for the latter, the transition occurs between 50 and 60 cm/s. Fig. 6 shows a summary of the experimental results for the two alloys. The transition from cellular to cell-free material is seen to occur at velocities roughly a factor of 2 less than the theoretical predictions. Such agreement is considered reasonable in view of the imprecise knowledge of the materials parameters required for the theory. A more complete discussion of these results occurs elsewhere [16].

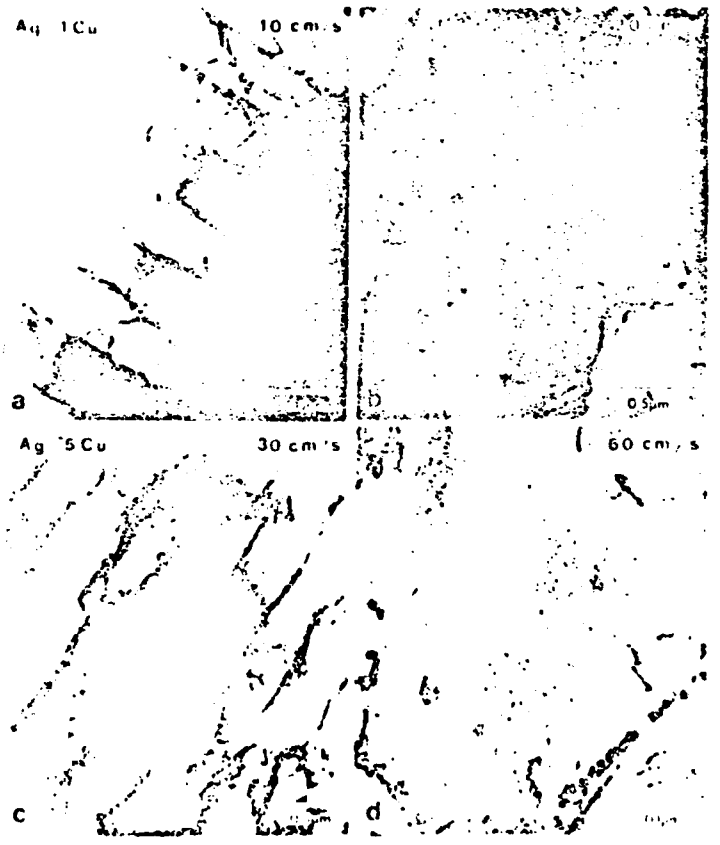

Fig. 5. a) Cellular and b) cell-free structures obtained in Ag-1 wt% Cu alloys rapidly solidified at 10 and 20 cm/s respectively. c) Cellular and d) cell-free structures obtained in Ag-5 wt% Cu alloys rapidly solidified at 30 and 60 cm/s respectively [16], TEM.

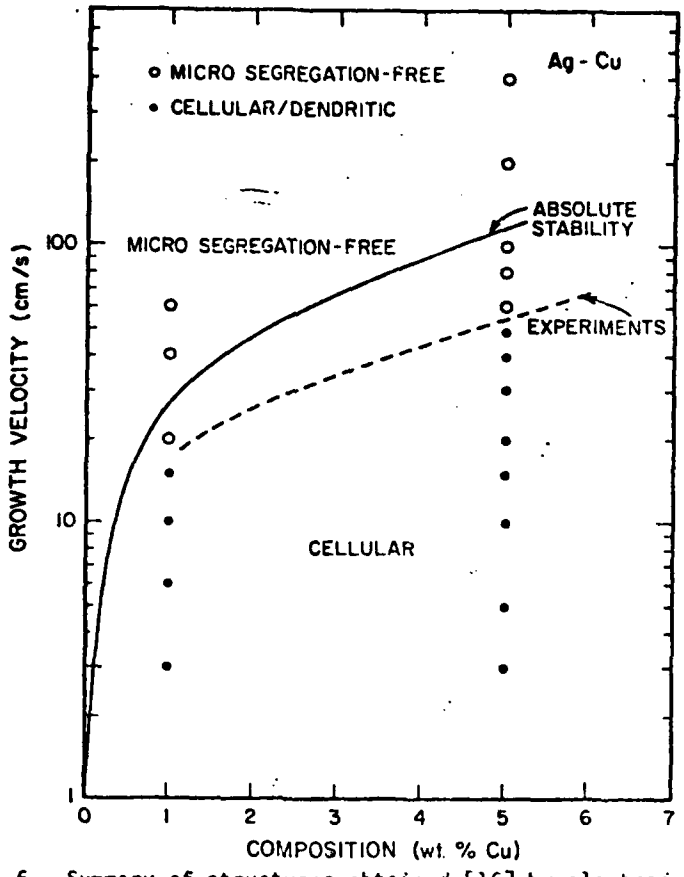

Fig. 6. Summary of structures obtained [16] by electron beam surface melting and resolidification of Ag-1 and 5 wt% Cu alloys at various growth rates. The comparison of the absolute stability theory with experiments is shown.

When the partition coefficient depends on the interface velocity, the stability theory must be modified [18]. This modified analysis of stability suggests the possibilty of increased instability of a planar liquid-solid interface, attributed to a feature called the "solute pump mechanism". Physically, the partition coefficient will vary across a perturbed solid-liquid interface because of local differences in velocity. This leads to a variation of the solute rejection rate along the interface and produces lateral solute segregation without the necessity of lateral diffusion. Hence perturbations with wavelengths much longer than those normally encountered at high growth velocity can occur and capillarity is less effective in stabilizing such perturbations. The results of the theory are complex and will only be described qualitatively here. It is found that the actual value of the partition coefficient can be substituted into the absolute stability equation only under certain conditions. If the rate of change of the partition coefficient with velocity is relatively small, and/or the absolute value of the rate of change of the interface temperature with respect to velocity is relatively large, this simple substitution method is valid. On the other hand, if the rate of change of the partition coefficient with velocity is large and/or the absolute value of the rate of change of the interface temperature with velocity is small, the simple substitution is not valid. Clearly the details of the size of these derivatives depends critically on the parameters β_0 and V_0 described in the previous section. Fig. 7 shows a plot of the demarcation between stability and instability for Ag-Cu alloys for a choice of β_0 of 10^{-2} s/cm and for various values of μ_T where $\mu_T = -\partial V/\partial T_I$. On the right side of the figure is shown the variation of the partition coefficient with velocity. On the left side is shown the demarcation between stability and instability. Depending upon the value of μ_T, the stability criterion can change dramatically.

It should be pointed out that the instability in the case of the "solute pump mechanism" is oscillatory in nature. This arises because of the temporal phase difference between the local velocity of the interface and the interface shape. Such oscillatory instabilities lead to microsegregation patterns that are three dimensional, whereas an ordinary microsegregation pattern is two dimensional (in directions transverse to the growth direction). Such oscillatory instabilities have not been observed, and only future experiments will determine their importance.

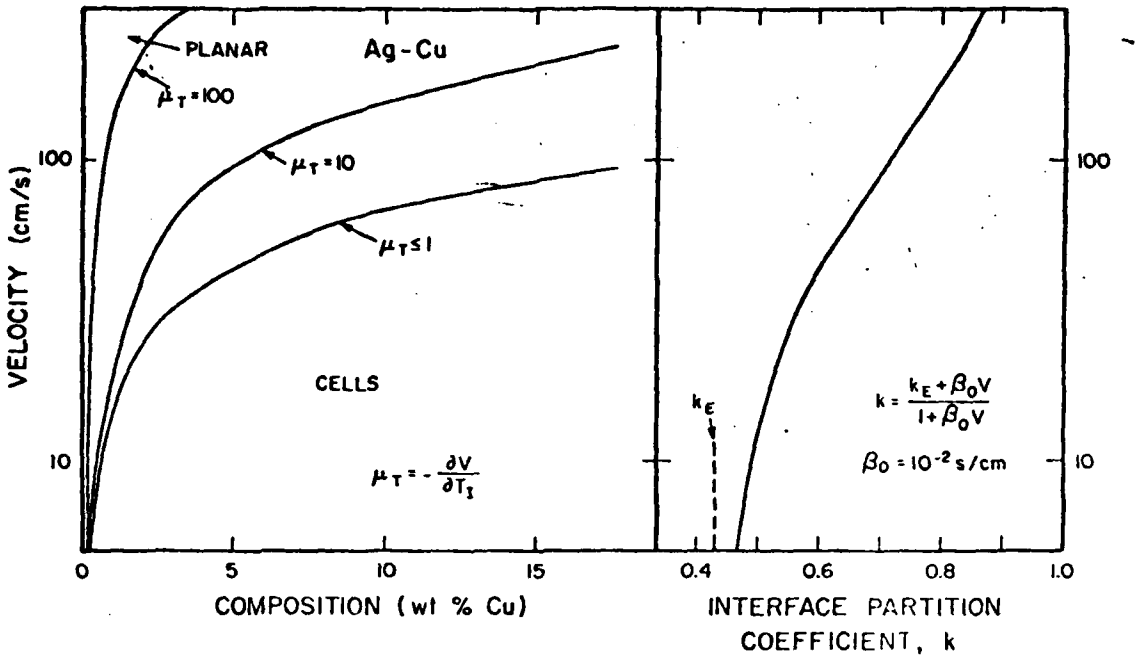

Fig. 7. Curves showing the onset of morphological instability for nonequilibrium conditions for which the partition coefficient, k, varies with V as shown on the right. Velocity for instability is shown as a function of the composition of bulk liquid for various values of the kinetic coefficient μ_T. For $\mu_T \leq 1$, the transition to instability is non-oscillatory in time and corresponds to a simple substitution of k(V) into the standard criterion for instability. The units of μ_T are cm/(Ks).

Concentrated Alloys

The solidification conditions required to produce microsegregation-free crystalline structures for concentrated alloys are generally associated with the temperature difference between the liquidus curve and the T_0 curve. For most terminal solid solutions, this difference increases with increasing concentration. The usual idea is that, compared to dilute alloys, such alloys require more rapid solidification or higher undercooling to produce microsegregation-free crystalline alloys. The simple trapping models presented earlier in this paper involve no explicit concentration dependence. Furthermore, a recent set of experiments conducted on Ag-rich Ag-Cu alloys [16-17], suggest that as the composition approaches the eutectic composition, the growth velocity required to form microsegregation-free structures decreases. At 15 wt% Cu, an interface velocity of approximately 2 m/s is required. At the eutectic composition (28 wt% Cu), a velocity of only 70 cm/s is required. Therefore, in this alloy, it is actually easier to form the microsegregation-free structure for the very concentrated alloys. Such results have several possible origins and one possibility is related to the dependence of the liquid diffusion coefficient on temperature, as discussed below.

The dependence of the liquid diffusion coefficient on temperature is generally neglected in ordinary solidification theory. Such is the case because of the fact that solidification almost always takes place very close to the liquidus temperature. Diffusion data is often described by an Arrhenius equation. For a melting point of 1000K and an activation energy of 10 kcal/mol, an undercooling of 300K will reduce the diffusion coefficient by an order of magnitude.

The dependence of the diffusion coefficient on temperature can affect substantially various ideas in solidification. In the following, it is assumed that the diffusion coefficient is only a function of temperature. The first example involves solute redistribution in the growth of concentrated alloys. In particular it has been noted previously [3] that the dependence of the diffusion coefficient on temperature can lead to a maximum in eutectic growth rate of approximately 10 cm/s. This maximum velocity has origins that are identical with the nose of the C curve for eutectoid growth observed in solid state transformations. Such a maximum eutectic growth rate is consistent with the fact that eutectic spacings are rarely observed to be finer than 200 A. A second example may occur in the stability theory. For planar growth with equilibrium at the solid-liquid interface, the interface temperature is at the solidus for the average alloy concentration. In many concentrated

alloys, the solidus may easily lie 300 K below the liquidus. An order of magnitude change in the diffusion coefficient can affect the prediction of the stability theory significantly. A third example involves a very simple modification of the trapping model presented previously. The parameter B_0 involves a diffusion coefficient. A simple approach to include composition dependence in a trapping theory would be to calculate the diffusion coefficient at the T_0 curve for various compositions. For pure silver, the diffusion coefficient is 2×10^{-5} cm^2/s at its melting point. For the eutectic composition the T_0 temperature is approximately 670 °C and the diffusion coefficient, based on an activation energy of 10 kcal/mole, is 6×10^{-6} cm^2/s. This simple idea leads to the conclusion that the growth velocity required for significant levels of solute trapping would be reduced by a factor of 3.5 as the composition changes from pure Ag to the eutectic composition. Such a trend is consistent with the observed data.

Conclusion

In this paper, a response function for the temperature of the interface during solute trapping has been discussed. This model for the temperature is consistent with thermodynamics and with models of solute trapping and collision limited growth. Such interface response functions should permit a rational approach to the solidification problem in a wide variety of conditions of heat flow and solute redistribution. Secondly, circumstances where the absolute stability equation can be used in lieu of the full stability theory have been addressed. Experimental results obtained by using electron beam surface melting of Ag-Cu alloys are consistent with the stability theory. Thirdly, a few comments have been presented on the conditions for microsegregation-free solidification of concentrated alloys. This area obviously remains ripe for experimental and theoretical investigation.

Acknowledgment

This work was partially sponsored by the Defense Advanced Research Projects Agency. One of us (RFS) received partial support from the National Science Foundation.

We would like to thank M. J. Aziz, J. W. Cahn, and D. Turnbull for helpful discussions.

References

[1] M. Cohen and R. Mehrabian, these proceedings.

[2] J. C. Baker and J. W. Cahn, in Solidification (ASM, Metals Park, 1971) p. 23.

[3] W. J. Boettinger, in Rapidly Solidified Amorphous and Crystalline Alloys, ed by B. H. Kear, B. C. Giessen and M. Cohen (Elsevier, 1982) p. 15.

[4] J. C. Baker, Interfacial Partitioning During Solidification, Ph.D. Thesis, MIT (1970) Chapter V. Also reported by J. W. Cahn, S. R. Coriell and W. J. Boettinger, in Laser and Electron Beam Processing of Materials, ed. by C. W. White and P. S. Peercy (Academic Press, NY, 1980) p. 89-103.

[5] M. J. Aziz, J. Appl. Phys. 53, 1158 (1982).

[6] K. A. Jackson, G. H. Gilmer, and H. J. Leamy, in: Laser and Electron Beam Processing of Materials, ed. by C. W. White and P. S. Peercy (Academic, NY, 1980) p. 104.

[7] R. F. Wood, Phys. Rev. B25, 2786 (1982).

[8] See, e.g., J. Narayan, J. Crystal Growth 59, 583 (1982).

[9] F. Spaepen and D. Turnbull, in Rapidly Quenched Metals, ed by N. J. Grant and B. C. Giessen (MIT Press, Cambridge, MA, 1976) p. 205.

[10] D. Turnbull and B. G. Bagley, in Treatise on Solid State Chemistry, ed. by N. B. Hannay (Plenum, New York, 1975) Vol. 5, p. 513.

[11] M. J. Aziz, these proceedings.

[12] J. L. Murray, Met. Trans. A, to be published.

[13] W. W. Mullins and R. F. Sekerka, J. Appl. Phys. 35, 444 (1964).

[14] S. R. Coriell and R. F. Sekerka, in Rapid Solidification Processing Principles and Technologies II, ed. by R. Mehrabian, B. H. Kear, and M. Cohen (Claitor, Baton Rouge, LA, 1980) p. 35.

[15] J. W. Cahn, S. R. Coriell, and W. J. Boettinger, in Laser and Electron Beam Processing of Materials, ed. by C. W. White and P. S. Peercy (Academic Press, New York, 1980) p. 89.

[16] W. J. Boettinger, R. J. Schaefer, F. S. Biancaniello, and D. Shechtman, Met. Trans. A, to be published.

[17] W. J. Boettinger, R. J. Schaefer, F. S. Biancaniello, and D. Shechtman, these proceedings.

[18] S. R. Coriell and R. F. Sekerka, J. Crystal Growth, to be published.

Rapid Solidification Processing: Principles and Technologies (III) edited by R. Mehrabian, NBS Internal Report (1983).

The Effect of Solidification Velocity on the Microstructure of Ag-Cu Alloys

W. J. Boettinger, R. J. Schaefer, F. Biancaniello

Metallurgy Division
National Bureau of Standards
Washington, DC 20234

and

D. Shechtman*

Center for Materials Research
The Johns Hopkins University
Baltimore, MD 21218

ABSTRACT

Electron beam surface melting and resolidification passes have been performed on a series of Ag-Cu alloys between 1 wt.% Cu and the eutectic (28.1 wt.% Cu) at speeds between 1.5 and 400 cm/s. At low growth rates conventional dendritic or eutectic structures are obtained. At high growth rates microsegregation-free single phase structures are obtained for all compositions. The velocity required to produce this structure increases with composition for dilute alloys and the values agree with the predictions of absolute stability of the liquid-solid interface with equilibrium partitioning. For alloys between 15 and 28 wt.% Cu, the velocity required to produce the microsegregation-free extended solid solution decreases with composition and is related to nonequilibrium trapping of solute at the liquid-solid interface. At intermediate growth rates for alloys with 9 wt.% Cu or greater, a structure consisting of alternate bands of cellular and cell-free material is obtained. The bands form parallel to the local interface.

Introduction

Rapidly solidified crystalline alloys are well known to exhibit a refined scale of microsegregation and interdendritic second phase particles. In some cases this microsegregation and the interdendritic phases can be completely eliminated by rapid solidification. These microsegregation-free structures can occur in alloys with compositions greater than the equilibrium solubility of the primary phase. Such structures provide an ideal starting microstructure for subsequent thermomechanical processing. However, the solidification velocities required to produce these structures are not well known.

The classic splat-quenching experiments of Duwez, Klement, and Willens [1] showed by x-ray diffraction that complete solubility of Ag and Cu in the solid state at all compositions could be obtained despite the presence of a solid miscibility gap and eutectic reaction in the phase diagram. Boswell and Chadwick [2] showed later by TEM examination that splat quenched Ag-Cu solidified from the melt as a single solid phase free of microsegregation. Surface melting and resolidification experiments using lasers or electron beams permit better control over solidification velocity than other rapid solidification techniques. Such experiments involve no bulk undercooling due to the presence of the alloy substrate and nucleation processes do not therefore play an important role. Also, because the liquid is contained in its own solid, a knowledge of heat transfer coefficients is not required. Elliott, Gagliano, and Krauss [3] using a pulsed laser, and Copley et al. [4-6] using a scanned CW laser, showed that supersaturated solid solutions of Ag-Cu could be formed by surface melting and resolidification experiments. The solutions however, contained a rather unique structure consisting of bands formed parallel to the local solidification interface. In these papers no structures are reported which are free of the bands and the velocities at which the transitions of microstructure occur are not described.

*Guest Worker, Metallurgy Division, National Bureau of Standards.

In the present paper, a series of electron-beam surface melting experiments has been performed on Ag-rich, Ag-Cu alloys. These experiments determine the transition velocity for changes from dendritic or eutectic growth to microsegregation-free solidification. This information permits the evaluation of existing rapid solidification models and points to areas where new models are required. The results and discussion in this paper appear in more detail elsewhere [7].

Experiments

Alloys were prepared by induction melting of 99.99 percent pure components in a graphite crucible and chill casting under argon in a carbon-coated copper slab mold. Ingots were cold-rolled to 3 mm thick sheets. For the surface melting experiments, the substrate must be prepared with either no microsegregation or microsegregation fine enough to ensure complete mixing during surface melting. Alloys containing 1 and 5 wt.% Cu were homogenized for 20 h at 750 °C. Alloys containing 9, 15, and 23 wt.% Cu were surface melted using overlapping electron-beam passes to a depth of ~ 0.5 mm at a scan speed of 3 cm/s. This produces a dendrite arm spacing less than 1 μm. Alloys containing 28.1 wt.% Cu (the eutectic composition) required no pretreatment. Wet chemical analysis of the six alloys yielded compositions of 1.07, 5.49, 9.23, 15.25, 23.50, and 28.61 wt.% Cu respectively. Rapid solidification experiments were performed by single, one-dimensional sweeps of a focused 21 keV, ~ 50 mA, ~ 1 mm diameter electron beam at speeds between 1.5 and 400 cm/s across the surface of a prepared alloy substrate which was attached to a water-cooled copper block.

Significant effects arise from the change in weld puddle shape as the scan rate is increased. The local solidification velocity is equal to the product of the scan velocity with the cosine of the angle between the scan direction and the local growth direction. Because of this factor, growth velocities even at the top center of the weld puddle for high scan speeds may differ from the scan speed. By examining longitudinal sections through the weld centerline by optical microscopy and assuming that grain boundaries propagate parallel to the growth direction, the angle, θ, between the electron beam scan direction and the growth direction at the top of the weld was measured. For scan speeds below 30 cm/s, the growth velocity near the weld surface usually differs from the scan speed by 15 percent or less. At velocities of 200 cm/s, the measurements indicated that the growth rate is about one-half of the scan speed.

Results

Figure 1 shows a summary of the microstructures observed at the center of the weld zone near the free surface as a function of the electron beam scan velocity and alloy composition for all experiments performed. The figure is divided into four regions exhibiting four general types of microstructure: (a) dendritic (cellular), (b) eutectic, (c) banded, and (d) microsegregation-free. The detailed results will be described by alloy composition.

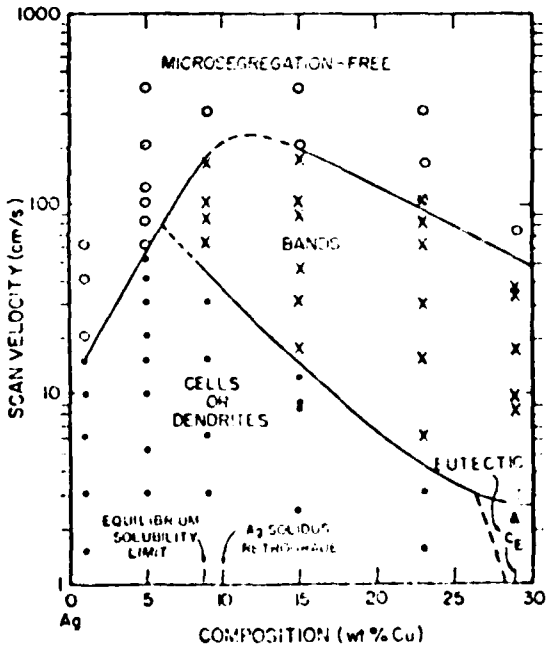

Fig. 1 Summary of microstructures observed in Ag-Cu alloys as a function of composition and electron-beam scan velocity.

Ag-1 wt.% Cu and -5 wt.% Cu.

Dilute alloys exhibit a transition from segregated to microsegregation-free structures at velocities which increase with alloy composition. These velocities agree within a factor of two with the theoretical predictions of absolute stability of the liquid-solid interface as described in another paper in these proceedings [8].

Ag-9 wt.% Cu, -15 wt.% Cu, and -23 wt.% Cu.

These alloy compositions are beyond the equilibrium solubility limit (8.8 wt.% Cu) of Cu in Ag at the eutectic temperature. The 9 wt.% Cu alloy does not exceed a calculated [9] Ag-solidus metastable retrograde composition however. As seen in figure 1, the microstructure of each of these alloys changes with increasing velocity from dendritic to banded and from banded to microsegregation-free.

The refinement of the primary arm spacing with scan velocity for Ag-9 wt.% Cu alloy is shown in figure 2. The rate of change of spacing with the actual solidification velocity may however be somewhat different due to changes in weld puddle shape as discussed previously. TEM examination of a Ag-15 wt.% Cu melt trail scanned at 2.5 cm/s showed a cellular microsegregation pattern with a relatively small volume fraction of eutectic in some areas and no eutectic in other areas (fig. 3). The maximum velocity at which dendritic growth is observed decreases with alloy composition from 30 cm/s for Ag-9 wt.% Cu to 4 cm/s for Ag-23 wt.% Cu (fig. 1).

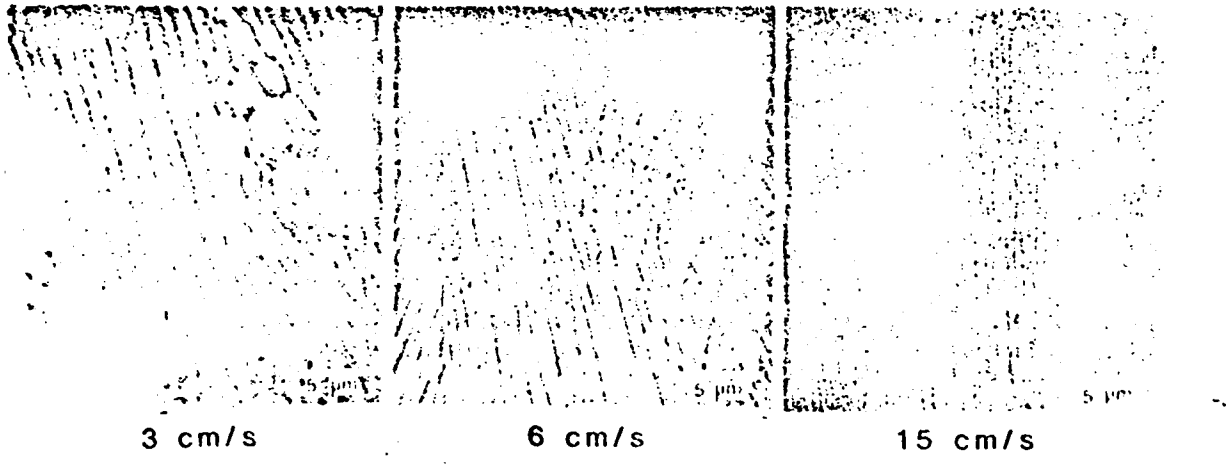

Fig. 2 Refinement of primary dendrite arm spacing with scan velocity for Ag-9 wt.% Cu alloys. SEM.

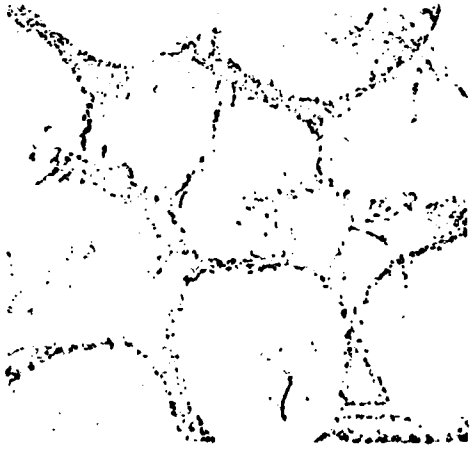

Fig. 3 Cellular microsegregation pattern observed in Ag-15 wt.% Cu alloy at a scan velocity of 2.5 cm/s. TEM.

A structure consisting of light and dark etching bands or striations is observed in the intermediate velocity range shown in figure 1. Figure 4 shows a transverse and a longitudinal section through the weld centerline for a 15 wt.% Cu alloy scanned at 30 cm/s. The lower part of the melted region, where the solidification velocity is lowest, is dendritic. The upper part of the melted region is banded. As seen in figure 4b the bands are parallel to the expected shape of the trailing edge of a melted zone. A transition from dendritic to banded structure, observed in the same sample suggests strongly that the origin of the banding phenomenon is growth related rather than an artifact of nonsteady beam power [3] or melt convection [5].

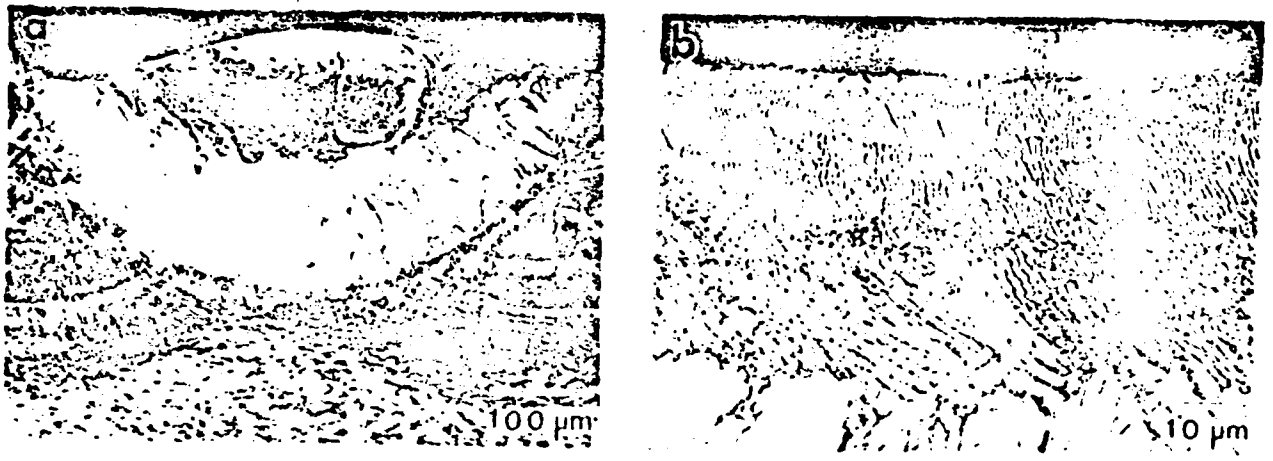

Fig. 4 (a) Transverse and (b) longitudinal sections of a Ag-15 wt.% Cu alloy scanned at 30 cm/s, showing transition from (unresolved) dendritic structure to the banded structure. Optical microscopy. The scan direction is to the right in (b).

TEM examination of the banded structure (fig. 5) in a 23 wt.% Cu alloy scanned at 17 cm/s revealed alternate layers of cellular and cell-free alloy. Evidently the dark etching material seen in optical micrographs of the banded structure corresponds to the cellular layer. X-ray fluorescence measurement in the STEM with a probe size just large enough to average over the entire width of an individual layer (~ 0.4 μm) revealed no statistically significant difference in average composition between the cellular and the cell-free layers. Clearly microsegregation does exist however within the cellular layers. Care was taken in the preparation of the TEM sample to document the growth direction. The cellular layer appears to originate microstructurally from an interface instability occurring in the cell-free layer. The cellular structure then propagates for a short distance until a layer of solute marks the cell fronts. The continuity between the cell-free layer and the subsequently formed cellular region is seen clearly in the isolated subgrain (dark grain). For higher scan velocities the widths of the cellular layers decrease compared to the widths of the cell-free layers, until at high velocity the cellular layers disappear and the banded structure is absent. In eutectic alloys, the banded structure is identical with the exception of a finer cell size.

Fig. 5 High magnification view of the banded structure. The growth direction is from lower right to upper left. TEM.

The 9 wt.% Cu, 15 wt.% Cu, and 23 wt.% Cu alloys are free of the banded structure at velocities of 300, 200, and 157 cm/s and above (fig. 1). As discussed in a previous section, actual growth rate may differ from the scan velocity because of changes in weld puddle shapes at scan velocities over 100 cm/s. Clearly however, the banded structure can be suppressed by high scan velocities to produce a microsegregation-free structure. Furthermore, this velocity decreases with increasing concentration. Figure 6 shows micrographs of a 23 wt.% Cu alloy scanned at 157 cm/s. The transition from a banded structure at the bottom of the melted region, where the growth rate is low, to a band-free structure at the top of the melted region, where the growth rate is high, is seen in figure 6b. TEM micrographs of this sample (fig. 6c) confirm the absence of bands but show significant solid state (spinodal) decomposition of the microsegregation-free structures produced from the melt.

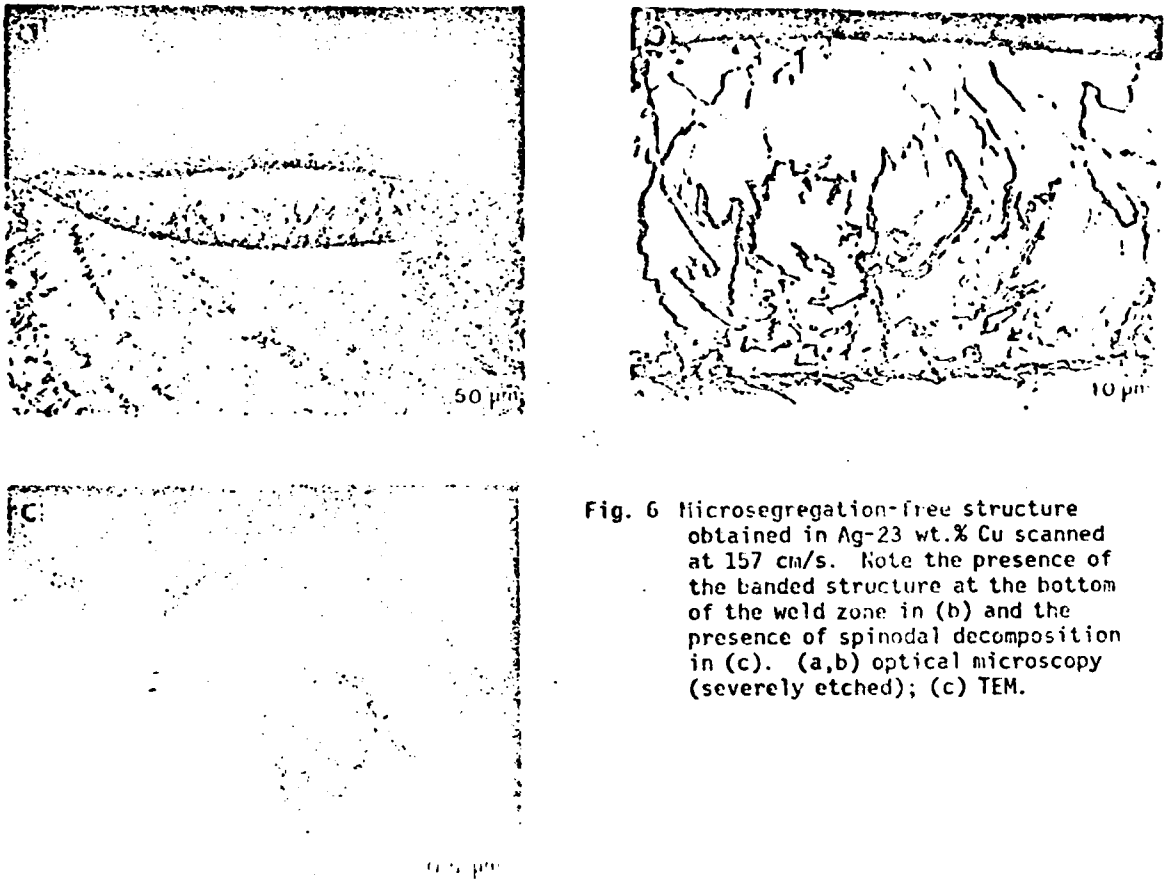

Fig. 6 Microsegregation-free structure obtained in Ag-23 wt.% Cu scanned at 157 cm/s. Note the presence of the banded structure at the bottom of the weld zone in (b) and the presence of spinodal decomposition in (c). (a,b) optical microscopy (severely etched); (c) TEM.

Ag-28 wt.% Cu.

The eutectic composition, when electron beam melted at 2.5 cm/s, consists of a fine eutectic structure with a spacing of ~ 200 Å. The electron diffraction pattern from the eutectic yields lattice parameters of 4.05 Å and 3.65 Å for the two phases. These values are close to those obtained [10] for Ag and Cu at their respective limits of equilibrium solid solubility at the eutectic temperature. Above 2.5 cm/s the eutectic composition does not solidify by a coupled growth mechanism. The microstructure consists of the same banded structure observed for noneutectic alloys. Above 70 cm/s the eutectic composition forms a structure without segregation similar to those shown in figure 6.

Discussion

Coupled Growth.

The maximum observed growth rate for the Ag-Cu eutectic in the present work is ~ 2.5 cm/s with a spacing of ~ 200 Å. Cline and Lee [11] have directionally solidified the Ag-Cu eutectic up to a growth rate of 0.27 cm/s with an average lamellar spacing of ~ 950 Å. In their experiments growth at higher velocities was prevented by the limitations of heat extraction in their solidification furnace. They found the lamellar spacing λ and the growth velocity, v, to be related by

$$\lambda^2 v = 1.4 \times 10^{-11} \text{ cm}^3/\text{s}. \quad (1)$$

In the present experiments, the heat extraction rate is not limited by a furnace. Extending their relation to a growth velocity of 2.5 cm/s predicts a lamellar spacing of 237 Å. This compares quite favorably with the eutectic spacing seen in the present work.

The present results strongly suggest that there should exist a theoretical limit on the rate at which coupled eutectic growth can occur. One theoretical limit can be found from the inclusion of a temperature dependent diffusion coefficient in eutectic growth theory [12]. The results of Eq. (1), phase diagram information and diffusion data [13] can be used to show that for slow growth, $v = 3.5 \times 10^{-4}$ (cm s^{-1} K^{-2})ΔT^2, where ΔT is the difference between the interface temperature and the eutectic temperature. Incorporating the temperature dependence of D to extend this relation to large undercooling, yields a maximum velocity of ~ 4.9 cm/s at a spacing of 78 Å. These estimates compare to the experimentally determined values of 2.5 cm/s at 200 Å. Possible reasons for this discrepancy and other theoretical limits on the eutectic growth rate are discussed elsewhere [7].

It should be emphasized that the temperature dependence of the diffusion coefficient becomes important in the present analysis only because of the relatively large undercoolings required to accomplish the solute redistribution and surface area creation necessary for eutectic growth. For dilute alloys the temperature dependence is much less important.

It is also interesting to note that the finest spacing seen by Boswell and Chadwick [2] in splat quench alloys was ~ 300 Å. This observation was used by them to assess the growth rate imposed by the splat quench on the foil. Because this eutectic structure occurred only in small regions adjacent to the metastable extended solid solution, it seems more likely that a maximum growth rate for the eutectic was reached locally in the small regions and surpassed in most of the foil to form the metastable structure.

Dendritic Growth in Concentrated Alloys.

To be consistent with the idea that a temperature dependent diffusion coefficient leads to a maximum rate for coupled growth of a eutectic, a maximum rate for dendritic growth of concentrated alloys must also exist. Although the theory of dendritic growth is continually being refined, especially for high rate [14], a simple expression formulated by Burden and Hunt for controlled growth [15] with the inclusion of a temperature dependent diffusion coefficient demonstrates the qualitative features of this maximum. The calculated maximum velocity [7] increases for increasing deviation from the eutectic composition. The maximum thus parallels the experimental data for the boundary between dendritic and banded microstructure. The calculated values are a factor of 2 to 4 higher than the experimental data, consistent with the disparity between the calculated and observed maxima for eutectic alloys. For very dilute alloys this maximum is irrelevant because it occurs at velocities above those at which the planar interface is stable.

Microsegregation-Free Structure.

For Ag-1 wt.% Cu and -5 wt.% Cu alloys, microsegregation-free structures are produced by planar growth at velocities predicted by absolute stability theory with equilibrium partitioning [8]. For concentrated alloys beyond the solidus retrograde composition, equilibrium partitioning is not a possible mechanism to produce a microsegregation-free structure. The transition from banded structure to microsegregation-free structure for concentrated alloys is most likely related to the onset of complete solute trapping. The upper velocity boundary of the banded region (fig. 1) when extrapolated to pure Ag suggests a velocity for solute trapping of ~ 5 m/s for dilute alloys. This velocity is consistent with data obtained for solute trapping in dilutely doped Si [16]. The fact that the

eutectic composition can be produced as a single phase microsegregation-free material at lower growth rates than, for example, 9 and 15 wt.% Cu alloys suggests a significant composition dependence for the onset of solute trapping.

Banded Structure.

The origins of the banded structure are difficult to determine with certainty. Beck, Copley, and Bass [6] have recently suggested that the bands are due to an instability proposed by Baker and Cahn [17] related to growth with solid composition and interface temperature above the solidus. However the observation of band-free structures in alloys for alloy composition beyond the solidus retrograde, where single phase growth can never occur below the solidus, seems to negate this idea.

The preceding discussion has suggested that the lower velocity boundary of the banded region in figure 1 is caused by a limitation of the maximum growth rate of dendritic and eutectic growth in concentrated alloys. The discussion also has suggested that the upper velocity boundary of the banded region in figure 1 is caused by significant deviation from interfacial equilibrium and the concommitant increase of the partition coefficient to unity. Clearly the microscopic events which occur during the formation of the banded structure must be related to these two phenomena. These microscopic events are discussed in more detail elsewhere [7].

Acknowledgment

The authors appreciate support from DARPA for this research. We also thank S. R. Coriell for many helpful discussions.

References

[1] P. Duwez, R. H. Willens, and W. Klement, Jr., J. Appl. Phys. 31, 1136 (1960).

[2] P. G. Boswell and G. A. Chadwick, J. Mat. Sci. 12, 1879 (1977).

[3] W. A. Elliott, F. P. Gagliano, and G. Krauss, Met. Trans. 4, 2031 (1973).

[4] S. M. Copley, M. Bass, E. W. Van Stryland, D. G. Beck, and O. Esquivel, Proc. III Int. Conf. Rapidly Quenched Metals, 1, p.147, The Metals Society, London (1978).

[5] D. G. Beck, S. M. Copley, and M. Bass, Met. Trans. A 12A, 16 (1981).

[6] D. G. Beck, S. M. Copley, and M. Bass, Met. Trans. A 13A, 1879 (1982).

[7] W. J. Boettinger, R. J. Schaefer, F. Biancaniello, and D. Shechtman, Met. Trans. A., to be published.

[8] W. J. Boettinger, S. R. Coriell, and R. F. Sekerka, these proceedings.

[9] J. M. Murray, Met. Trans. A, (1983) to be published.

[10] R. K. Linde, J. Appl. Phys. 37, 934 (1966).

[11] H. E. Cline and H. Lee, Acta Met. 18, 315 (1970).

[12] W. J. Boettinger, in Rapidly Solidified Amorphous and Crystalline Alloys, B. H. Kear, B. C. Giessen, and M. Cohen, Eds., Elsevier, p. 15 (1982).

[13] T. Yamamura and T. Ejima, J. Jap. Inst. Met. 37, 901 (1973).

[14] R. Trivedi, to be published.

[15] M. H. Burden and J. D. Hunt, J. Cryst. Growth 22, 109 (1974).

[16] M. J. Aziz, J. Appl. Phys. 53, 1158 (1982).

[17] J. C. Baker and J. W. Cahn, in Solidification, ASM, Metals Park, p. 23 (1971).

Presented at the Third Conference on Rapid Solidification Processing: Principles and Technologies, National Bureau of Standards, Gaithersburg, Md., U.S.A. December 6-8, 1982.

NONDESTRUCTIVE CHARACTERIZATION OF RAPIDLY SOLIDFIED Al-Mn ALLOYS

R. J. Schaefer*, M. Rosen**, J. J. Smith**, D. Shechtman** and R. Mehrabian*

*National Bureau of Standards
Washington, DC 20234

**The Johns Hopkins University
Baltimore, MD 21218

ABSTRACT

Supersaturated Al-Mn alloys were prepared by melt spinning and by electron beam surface melting of bulk samples. The samples were evaluated by several methods, in the as-prepared condition and after annealing for several different times at 450° C. The measurements gave consistent indication of the high degree of supersaturation attained in the rapidly solidified materials, and showed the changes of several properties as precipitation progressed. At low supersaturation the precipitates were localized at the grain boundaries and the supersaturation of the lattice disappeared only slowly, whereas at higher manganese concentrations the precipitates were abundantly dispersed throughout the matrix and the lattice supersaturation decreased more rapidly.

Introduction

Nondestructive methods are needed to characterize the modified layers which can be generated by the action of directed energy sources on the surface of metals. The information generally required includes the depth of the layer and its microstructural character. In many cases the surface layer will not differ in composition from the bulk material, i.e. no surface alloying is present, and the surface layer is detected through the effect of the modified microstructure on the probing signal.

Manganese has a maximum equilibrium solid solubility in aluminum of approximately 1.55 wt.% at the eutectic temperature [1], which is only slightly below the melting temperature of aluminum. It has long been known [2], however, that this solubility can be increased by rapid solidification to compositions far beyond the eutectic (2%) between Al and Al_6Mn. In response to heat treatment, precipitation may occur as either the equilibrium orthorhombic Al_6Mn or other phases [3] depending upon the temperature and impurity content. Nondestructive evaluation of the state of precipitation may either detect some direct influence of the precipitates or it may primarily detect the decrease of Mn in solid solution as the process progresses.

Results and Discussion

Sample Preparation

Melt-spun ribbons with Mn concentrations of 0.1, 1, 2, 3, 7, 9, 12, and 15 wt.% Mn were prepared from 99.999% Al and 99.95% Mn. The ribbons were typically 2 mm wide and 20 μm thick. For annealing, the ribbons were sealed in borosilicate glass ampoules with 1/2 atmosphere of helium. Annealing was at 450°C for 5 minutes, 1 hour and 3 hours.

A sample of Al-7 wt.% Mn was prepared for electron beam surface melting by chill casting, rolling at 600°C to a thickness of 9 mm, and annealing for 1 hour at 450°C. Surface melting was carried out by electron beam scans along the length of the sample at a velocity of 50 cm/s, with successive scans offset 0.4 mm laterally and with a time delay of 15 seconds between scans to allow cooling. In this way a rapidly solidified surface layer 8 cm long, 2 cm wide and 0.2 mm deep was formed.

Sample Evaluation

The melt-spun ribbons were evaluated by measurements of lattice parameter, electrical resistivity, and sound velocity, and by transmission electron microscopy. The measurements indicated that

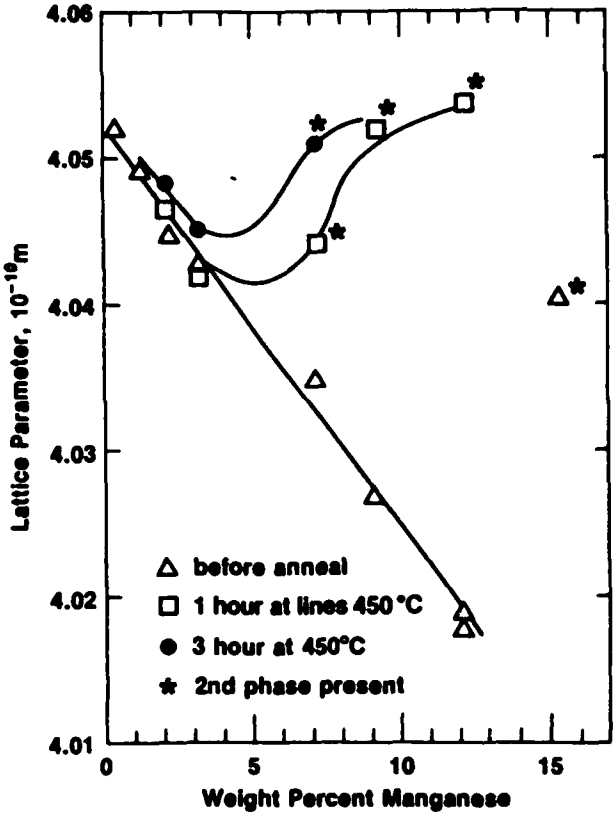

Fig. 1. Variation of the lattice parameter of the Al phase as a function of Mn concentration in the as-spun and annealed conditions.

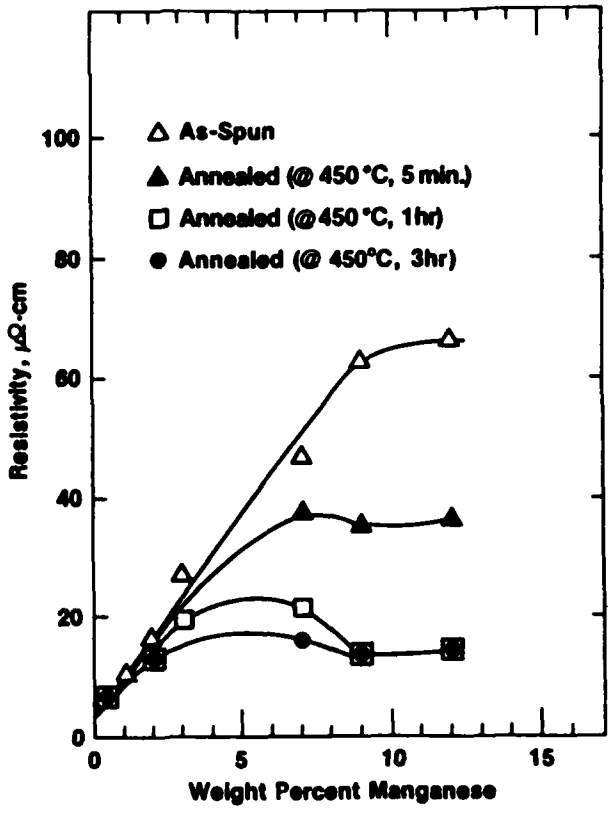

Fig. 2. Variation of the electrical resistivity in Al-Mn alloys as a function of Mn concentration in the as-spun and annealed conditions.

at concentrations up to 12 wt.% most of the manganese was in solid solution in the as-spun ribbons. At 450°C, precipitation occurs heterogeneously at the grain boundaries at low Mn concentrations but at many more locations throughout the sample at high concentrations. As a result, the supersaturation of manganese in the aluminum lattice diminishes rapidly in the high concentration samples but more slowly in the more dilute alloys where longer-range diffusion is required.

Lattice Parameter Measurements

Lattice parameters were measured on an X-ray diffractometer using CuK_α radiation, plotting calculated values for individual peaks against $Y = (\cos^2\theta/\sin\theta)$ and extrapolating to $Y = 0$. In the as-spun ribbons, diffraction peaks were seen only from the aluminum phase at compositions up to 12 wt.% Mn, and the lattice parameter (Fig. 1) decreased linearly with increasing Mn content, with a slope in agreement with prior measurements [2,3]. At 15 wt.% Mn, additional peaks, not corresponding to the equilibrium Al_6Mn phase, appeared in the pattern and the lattice parameter of the Al phase indicated a composition of approximately 4 wt.% Mn in solution. Measurements of the top and bottom surfaces of the 12% alloy showed essentially identical results, indication that the supersaturated phase was present throughout the thickness of the ribbons.

Annealing of the Al-7 wt.% ribbon for 1 hour at 350°C showed little change in the diffraction pattern. After 1 hour at 450°C however, Al_6Mn was present and the peaks from the aluminum phase were significantly broadened, with the average value of the aluminum lattice parameter having increased approximately one half of the way to its equilibrium value at that temperature. At 9 and 12

wt.% Mn, the 1 hour 450°C anneal gave an aluminum phase lattice parameter close to the equilibrium value but at 3 wt.% Mn or less the same anneal gave no perceptible change in the lattice parameter. Annealing for 3 hours brought the lattice parameter of the 7wt.% Mn sample close to its equilibrium value and also caused significant changes in the low composition samples.

The diffraction chart of a 9 wt.% Mn sample annealed for 5 minutes at 450°C showed extreme line broadening with a line shape indicating that much of the aluminum phase was still close to its original composition but that localized regions had already become significantly depleted in manganese.

The Al-7 wt.% Mn sample prepared for surface melting showed initially a lattice parameter for the aluminum phase indicating only a small concentration of Mn in solution, and strong Al_6Mn peaks. After electron beam surface melting, only a single faint peak indicative of a second phase was present and the measured lattice parameter of the aluminum phase lay well below the line for as-spun ribbons in Fig. 1. The value of the lattice parameter in this case, however, may have been seriously affected by the large residual stresses which are inevitably present in such surface melted layers. The surface layer showed a pronounced orientation texture as revealed by the complete absence of the (111) and (222) peaks in the diffraction pattern.

Electrical Resistivity

The electrical resistivity of the ribbons (Fig. 2) was determined by means of a standard four probe potentiometric method with an accuracy of about 1 part in 10^5. Considering the overall uncertainty in the geometrical shape factor of each sample, the estimated error in the absolute resistivity values is about ±5%. The as-spun ribbons exhibit a strong increase in electrical resistivity with increasing manganese content. An apparent leveling of the resistivity is observed at concentrations above 9 wt.% Mn. Annealing at 450°C for even short periods (5 minutes) has a large effect on the electrical resistivity of the higher concentration alloys. By means of a nucleation and diffusion controlled process, Al_6Mn particles are precipitated out of the aluminum matrix, thus denuding the lattice of effective scatterers of electrons. This "purification" process is apparently responsible for the observed decrease in electrical resistivity relative to the supersaturated, as-spun, alloy. The difference in the absolute values of the electrical resistivity between the as-spun and annealed condition, $\Delta\rho$, increases with increasing manganese concentration up to 9 wt.% Mn, and subsequently levels off. The electrical resistivity of the annealed 12 wt.% Mn alloy is almost identical to that of the 2 wt.% Mn alloy, indicating that the contribution of the fully grown, and incoherent, Al_6Mn precipitates to the measured total resistivity is almost negligible. Such a behavior is expected from relatively large isolated precipitates, about 5×10^{-7}m in size, in a continuous matrix phase, in which case the resistivity of the sample is determined primarily by the resistivity of the matrix.

Electron Microscopy

The microstructures of as-spun and annealed ribbons of the 3 wt.% and 9 wt.% Mn alloys are shown in Fig. 3. The 3 wt.% Mn alloy shows only dislocations in the as-spun condition, and after 1 hour at 450°C it shows a few Al_6Mn precipitates localized at grain boundaries. In the Al-9 wt.% Mn alloy, the as-spun alloy consists of a cellular structure with very fine precipitates at the cell boundaries. It is conjectured that the fine precipitates were formed in the solid state during rapid cooling after solidification. It is not clear whether the fine precipitates are direct precursors of the large ones that form upon annealing at 450°C. After 1 hour at this temperature, the 9 wt.% Mn sample shows abundant Al_6Mn precipitates throughout.

X-ray, TEM and electrical resistivity observations all indicate that at high supersaturations precipitation progresses most rapidly because of the large number of nuclei formed and the correspondingly short diffusion distances. The leveling of the electrical resistivity at concentrations above 9 wt.% Mn may be the result of the presence of the cellular structure. It is suggested that the concentration of Mn in the Al lattice adjacent to the cell boundaries is very low, and in this case these regions would act as a continuous network of low-resistivity material which would decrease the electrical resistivity of the sample to a larger extent than a simple volume fraction would indicate. The x-ray diffraction peaks of the Al-12 wt.% Mn ribbons have distinct tails on the low angle side, confirming that some aluminum is present with considerably less than 12 wt.% Mn in solution.

Sound Wave Velocity

The velocity V_e of ultrasonic extensional waves is $(E/\rho)^{1/2}$, where E is the Young's modulus and ρ is the density. The velocity of such waves propagating along the ribbon was determined by measuring the transit time of a single pulse generated by a laser and detected by a piezoelectric transducer. The detector was about 200 mm from the spot on the ribbon irradiated by the Q-switched Nd:YAG laser (Fig. 4). The transit time of the extensional sound wave propagating along the ribbon

Al-3 Wt. % Mn

No segragation is observed in the as-spun ribbon. Following heat treatment, large Al_6Mn precipitates form at the grain boundaries.

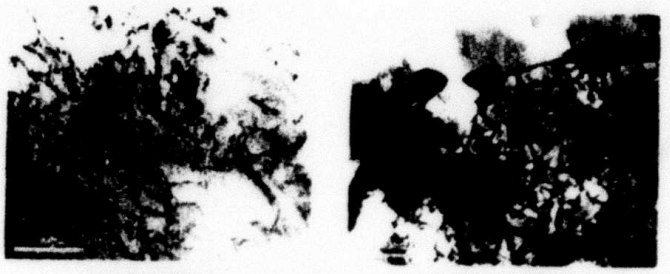

Al-9 Wt. % Mn

Fine particles of metastable compound form at the grain boundaries of as-spun ribbon. Following heat treatment, precipitation of Al_6Mn is observed.

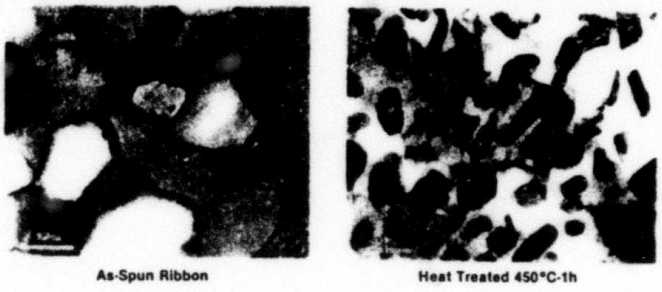

Fig. 3. TEM of Al - 3 wt.% Mn and Al - 9 wt.% Mn in the as-spun and annealed conditions.

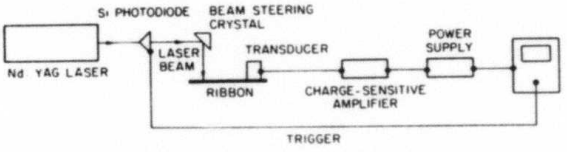

Fig. 4. Laser generation and piezoelectric detection of ultrasonic waves in thin ribbons.

could be determined to within one part in 10^5. The separation between the impinging laser pulse and the quartz receiver was determined to within ± 0.2 mm. The total estimated error in the calculated value of the sound velocity was ± 0.1%. The measurements were carried out at room temperature in the as-spun condition and after the ribbons were subjected to the appropriate heat treatments.

The propagation velocity of Rayleigh surface waves was used to characterize the supersaturated solid solution generated by electron beam surface melting of the slab of Al-7 wt.% Mn. The Rayleigh velocity in the electron beam melted and rapidly solidified layer was found to be 3039 m/s. On the untreated side of the slab, the microstructure of which consisted of Al_6Mn precipitates in an aluminum phase matrix, the Rayleigh wave velocity was 3091 m/s, substantially higher than the velocity in the supersaturated solid solution. This behavior was expected since the specific sound velocity of the Al_6Mn particles is substantially higher than that of the aluminum matrix. A similar behavior was observed in Al-Cu alloys after aging [5].

Figure 5 shows the variation of the sound velocity in Al-Mn alloys as a function of Mn content for both as-spun and annealed alloys. The salient feature in Fig. 5 is the fact that the sound velocity, and thus the Young's modulus, of the heat treated alloy is always higher than that of the

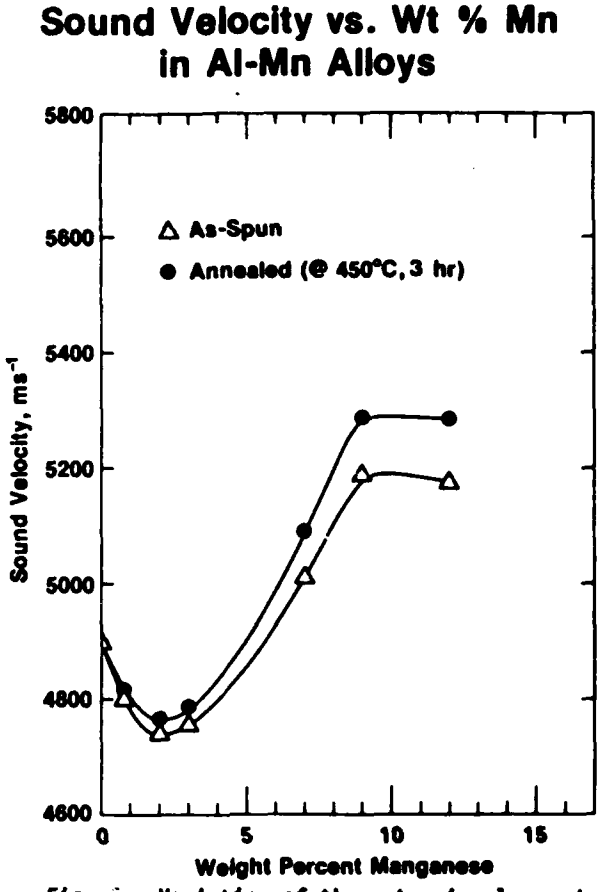

Fig. 5. Variation of the extensional sound wave velocity in Al-Mn alloys as a function of Mn concentration in the as-spun and annealed conditions.

as-spun state. The difference between the as-spun and the annealed conditions increases with increasing Mn concentration, up to 9 wt.% Mn. This relatively large difference is significant when nondestructive techniques are considered for monitoring on-line and in real-time the progress of the metallurgical process leading to a rapidly solidified single-phase supersaturated alloy.

The extensional sound wave velocity initially decreases with increasing Mn content up to about 2 wt.% Mn. Subsequently the velocity increases, followed by a plateau starting at 9 wt.% Mn. The density, based on the measured lattice parameters of the as-spun ribbons, is expected to be a linear function of composition. Reported values of the static elastic modulus as a function of composition [6] show a slight suggestion of nonlinearity, but not enough to account for the pronounced minimum in sound velocity seen here. It is thus apparent that either the density of the melt-spun ribbons differs from the value derived from X-ray measurements, or the elastic modulus of the ribbons differs from that measured statically on bulk samples.

CONCLUSIONS

Nondestructive ultrasonic and electrical resistivity measurements were found to be feasible for in-process dynamic monitoring and determination of the supersaturation range of rapidly solidified alloys. Up to 12 wt.% Mn can be incorporated into an Al lattice by rapid solidification, and the subsequent precipitation can be monitored by any of several methods.

ACKNOWLEDGEMENTS

The authors thank F. S. Biancaniello for sample preparation and C. Bechtold for consultation on X-ray diffraction. Thanks are also due to DARPA for financial support.

REFERENCES

[1] F. A. Shunk, Constitution of Binary Alloys, Second Supplement, McGraw-Hill, New York (1969)
[2] G. Falkenhagen and W. Hofman, Z. Metallkunde 43, 69 (1952)
[3] R. Hofer, S. E. Naess, and E. Nes, Z. Metallkunde 64, 640 (1973)
[4] I. Obinata, E. Hata, and K. Yamagi, J. Japan Inst. Met. 17, 496 (1953)
[5] M. Rosen, E. Horowitz, S. Fick, R. Reno and R. Mehrabian, Mater. Sci. Eng. 53, 163 (1982)
[6] N. Dudzinski, J. R. Murray, B. W. Mott, and B. Chalmers, J. Inst. Metals 74, 291 (1948)

Presented at the Third Conference on Rapid Solidification Processing: Principles and Technologies, National Bureau of Standards, Gaithersburg, Md., U.S.A. December 6-8, 1982.

THE MICROSTRUCTURE OF RAPIDLY SOLIDIFIED NiAl-Cr QUASIBINARY EUTECTIC

D. Shechtman*, T. Z. Kattamis+, F. S. Biancaniello++ and W. J. Boettinger++

*Center for Materials Research
The Johns Hopkins University
Baltimore, MD 21218

+Dept. of Metallurgy
University of Connecticut
Storrs, CT 06268

++Metallurgy Division
National Bureau of Standards
Washington, DC 20234

ABSTRACT

The microstructure of melt-spun ribbon of the NiAl-Cr quasibinary eutectic composition has been characterized by optical and transmission electron microscopies. The eutectic composition is Ni-38.5wt%Cr-19.4wt%Al and is of interest because of the similarity of crystal structures (CsCl for β-NiAl and BCC for α-Cr) and lattice parameters of the two phases in the eutectic. The rapidly quenched microstructure consists of 0.5 μm diameter columnar grains of the β-NiAl phase supersaturated with chromium to the eutectic composition. Between these grains a fine rod-type eutectic structure of the β-NiAl and α-Cr phases is observed with eutectic spacings as fine as 12 nm. The composition of the phases in the eutectic portion of the microstructure were found to be close to the equilibrium solubilities for these phases. A rationale for the appearance of a supersaturated β-NiAl phase at the eutectic composition, rather than a supersaturated α-Cr phase, will be presented based on the T_o curves for this alloy system.

Introduction

The directional solidification of NiAl-Cr quasibinary eutectic alloy (Ni-33at%Al-34at%Cr) was previously investigated by Walter, et al. [1-4], who saw in it potential for high temperature applications. The eutectic consists of fine, nonfaceted fibers of α-Cr BCC phase embedded in a β-NiAl matrix, which is an ordered BCC phase (CsCl-type) containing some chromium in solid solution. From previous work by Kornilov, et al. [5], the NiAl-Cr quasibinary eutectic temperature is 1445 °C. The α-Cr phase at 1200 °C contains 20.6 mole% NiAl and, hence, has a composition of 17.1at%Ni-17.1at%Al-65.8at%Cr. The β-NiAl at 1200 °C phase contains 84.5 mole% NiAl, hence has a composition of 45.8at%Ni-45.8at%Al-8.4at%Cr. The volume fraction of fibers is about 0.34. In the directionally solidified eutectic all directions and planes of the two phases are parallel. The solidification microstructure consists of eutectic colonies of α-fibers of circular cross-section embedded in <100>-oriented columnar grains of β-NiAl and parallel to the growth direction, except near the cell boundaries where they are inclined to this direction. Despite this inclination the crystallographic relationship between fibers and matrix remains the same [1]. Both cubic phases are crystallographically related with only a small lattice mismatch, as evidenced by the large distance between dislocations observed at the interphase interface.

Walter, et al. [2] studied the effect of growth velocity on inter-fiber spacing. They quantitatively established the decrease in cell size and inter-fiber spacing with increasing growth velocity. They also investigated the effect of alloy additions on microstructural changes, in particular the rod-to-plate transition [3].

It appeared interesting to extend the study of solification microstructures of the NiAl-Cr quasibinary eutectic to those achieved by rapid solidification, anticipating that the small difference in lattice parameter between the two phases would lead to substantial extension in solid solubility. Melt-spinning was used in this investigation. The growth rates achieved in this process are difficult to quantify, because of the possibility of bulk undercooling and an imprecise knowledge of the interface heat transfer coefficient. However, melt-spinning provides a simple way to assess

the alloy's response to rapid solidification processing.

Results of the work on microstructure of melt-spun ribbon of NiAl-Cr quasibinary eutectic alloy are reported herein and are also included in another publication [6].

Experimental Procedure

Rapidly solidified ribbons of NiAl-Cr quasibinary eutectic were melt-spun on a room temperature wheel in a helium atmosphere. Ribbons of about 25 μm thick and 2.5 mm wide were obtained at a linear velocity of 24 m/s. The ribbons were studied by optical microscopy, X-ray diffraction and analytical electron microscopy. Specimens for electron microscopy were electropolished and studied in a scanning transmission electron microscope equipped for nondispersive X-ray fluorescence analysis. The composition of the phases in the foil was evaluated by using the nominal composition of the specimen as standard. The Cliff-Lorimer coefficients were determined by using the intensities obtained from a thin area representing the general microstructure with a probe size of about 1 μm. Analysis of individual phases was then conducted in the same area of similar thickness. The C-L coefficients were redetermined for each set of analyses in different regions of the foil. This procedure eliminates the need for additional corrections of the measured X-ray intensities.

Results

The microstructure of an arc-melted chill-cast cylindrical specimen, 6.3 mm in diameter is illustrated in Figure 1. The rod-like α-Cr-rich phase is revealed as the dark etching phase.

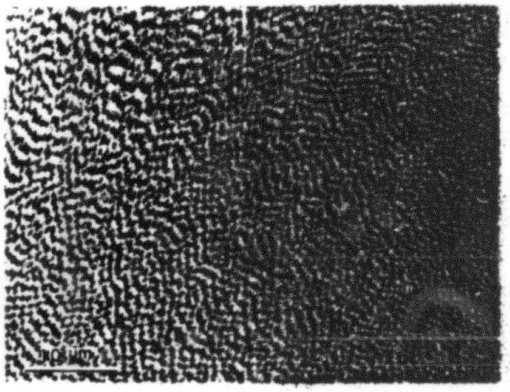

Figure 1: As-cast microstructure of arc-melted NiAl-Cr quasibinary eutectic (optical microscopy).

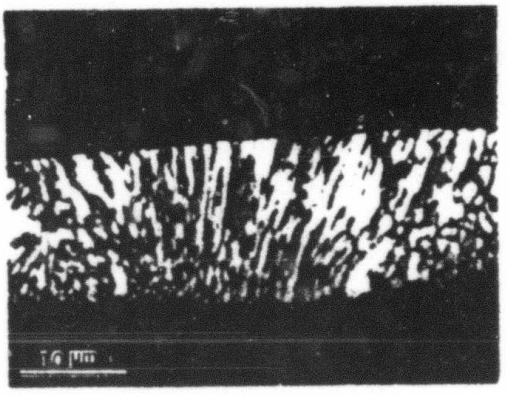

Figure 2: Columnar grains in melt-spun ribbon, edge-on section (optical microscopy).

The cast microstructure of the ribbons consists mainly of a columnar zone with columnar grains parallel to the heat flow direction. The intergranular spaces were not optically resolved. The average columnar grain width increased slightly with distance from the chill, Figure 2, from about 0.5 to 1.3 μm. The average columnar grain width also increased slightly with ribbon thickness.

The microstructure of the ribbon as observed by electron microscopy is shown in Figure 3, which represents cross-sections of columnar grains that grew perpendicular to the ribbon surface. The columnar grains average 0.5 μm in diameter and are surrounded by a fine eutectic. The boundary between a columnar grain and a region of particularly fine eutectic is shown at a higher magnification in Figure 4. The columnar grain is decomposed into a fine microstructure typical of conditional spinodal decomposition [7] with an average wavelength of 10 nm (lower right, Figure 4). The eutectic rods grow roughly perpendicular to the columnar grain and their spacing ranges from 12 nm, Figure 4, to 60 nm, Figure 3. The microstructure is not uniform and in some areas the volume fraction of the columnar grains by far exceeds that of the eutectic, Figure 5. In other regions of the same foil the volume fraction of the eutectic is much higher, Figure 6. These variations may correspond to different distances from the heat sink, however this was not confirmed in the present study.

A large proportion of columnar grains are single ordered domains. However, some of them contain two or more domains. Anti-phase domain boundaries are shown in Figures 3 and 7. These APBS run across the grain and in most cases end in a chromium-rich rod of the eutectic. The significance of these APBS to the understanding of the solidification process will be discussed later in this paper.

A diffraction pattern taken from a columnar grain, Figure 8, identified the structure as CsCl (B2). A diffraction pattern taken from a columnar grain and its surrounding eutectic, Figure 9, shows no extra reflections besides the CsCl. This indicates that both phases in the eutectic and

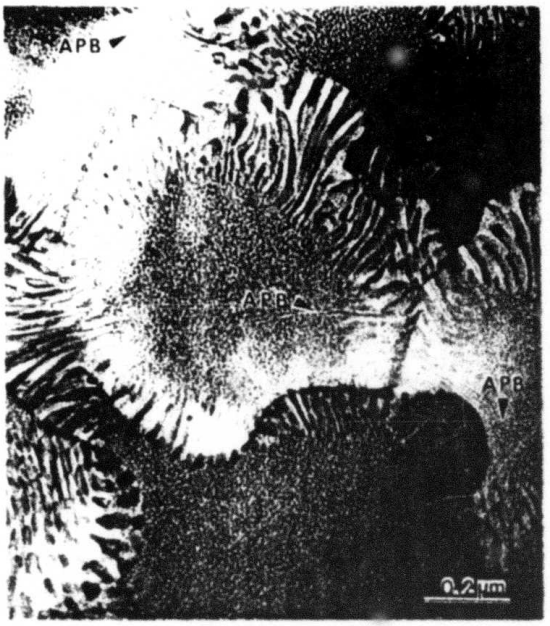

Figure 3: Transverse section of columnar grains and surrounding eutectic in melt-spun ribbon (TEM). Note APBS in center grain.

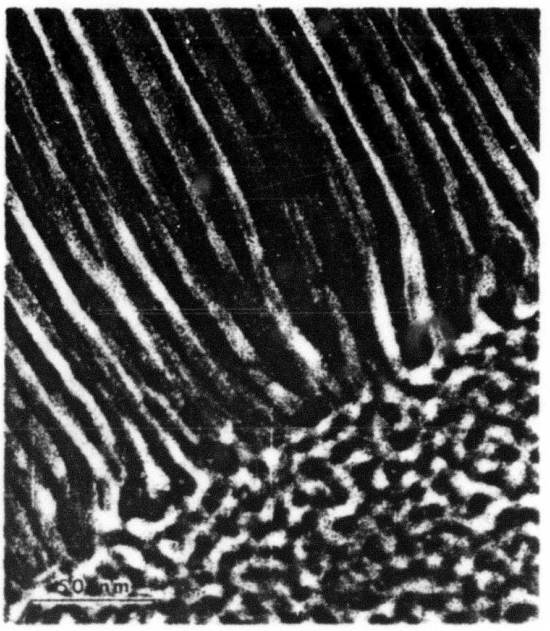

Figure 4: Columnar grain-eutectic interface. Inter-rod eutectic spacing: 12 nm (TEM).

Figure 5: Region of foil consisting primarily of columnar grains (TEM).

Figure 6: Region of foil consisting primarily of eutectic (TEM).

the columnar grain have the same orientation and almost identical lattice parameters. An X-ray diffraction scan taken from the ribbon shows that the reflections from the CsCl lattice and those from the BCC lattice are indistinguishable. Lattice parameter measurements resulted in a figure of a = 0.28882 nm. Microdiffraction patterns were taken from a rod and the adjacent matrix of the eutectic, as shown in Figure 10. The rod is identified as BCC, Figure 10a, the matrix as CsCl structure, Figure 10b.

A composition analysis of the columnar grain cores has shown that they have the same composition

as the original alloy, Figures 11a and b. They are, therefore, β-NiAl supersaturated with chromium to the eutectic composition. The BCC phase in the eutectic was also analyzed, Figure 11c and was found to be composed mainly of chromium of near equilibrium composition at the eutectic temperature (13.9 at%Ni and 7.5 at%Al). The CsCl phase in the eutectic was not analyzed due to experimental difficulties, but based on an estimated volume fraction of the phases in the eutectic the phase is estimated to contain about 13 at% chromium, i.e. near the expected equilibrium composition for the β-NiAl phase at the eutectic temperature.

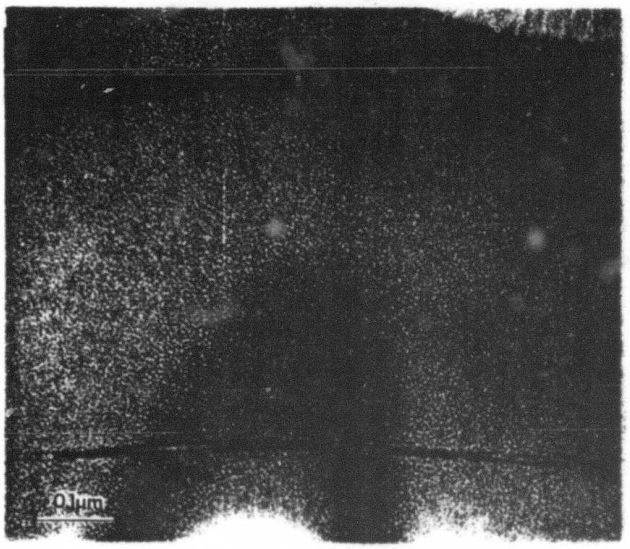

Figure 7:

High magnification illustration of APBS

Discussion

Two features of this rapidly solidified structure are unique and will be discussed separately: The columnar grains of spinodally decomposing alloy with the β-NiAl structure and with composition near the eutectic, and the fine rod-type eutectic structure. It is important for the analysis of rapid solidification processes to establish whether the β-NiAl phase was a direct product of solidification or whether it has ordered in the solid state from a supersaturated α-Cr phase.

Columnar Grains

Because of the extension of solubility required for the formation of the columnar grains, an examination of the possible T_0 curves for the NiAl-Cr system is in order. Figure 12 shows the stable phase diagram as solid lines [5] and a possible schematic set of metastable extensions of the solvus curves (dashed) and the T_0 curves (long-short dashed). The figure assumes that the two solvus curves meet at a metastable tricritical point above which the transition from the BCC phase to the CsCl phase is second order. This transformation can be second order according to the symmetry restrictions of Landau [8]. This metastable extension upward to the tricritical point, where the crystal structures differ by an ordering reaction, is formally similar to the metastable extension of the solvus curves between identical crystal structures (FCC) in the Ag-Cu system upward to an ordinary critical point. The proposed metastable tricritical point is thermodynamically identical to the stable tricritical point in the Fe-Al system where the ordering is between Fe (BCC) and FeAl (B2) [7]. The schematic free energy curves for the solid phases shown in Figure 12 are identical to those proposed by Allen and Cahn [7]. With the addition of the liquid free energy curve to generate the stable eutectic phase diagram the structure of the T_0 curves becomes apparent. In this figure we have assumed that the tricritical temperature is relatively low due to the similarity in the lattice parameters of β-NiAl and α-Cr. The lattice parameters would be identical above the tricritical point. In Figure 12 the dotted curve is the metastable extension of the second order phase transition below the tricritical point and is the locus of points where the free energy curves of the disordered and ordered phases join tangentially. This curve is generally thought to lie much closer to the solvus for the disordered phase rather than that for the ordered phase [7]. The T_0 curve for the disordered phase is seen to split into two branches when it crosses this dotted line. The lower branch is the continuation for the disordered phase, while the upper branch is for β-NiAl phase. This upper branch continues to the NiAl side of diagram where it is the normal T_0 curve for β-NiAl. The relatively small depression of the T_0 curve for β-NiAl below the eutectic temperature is a

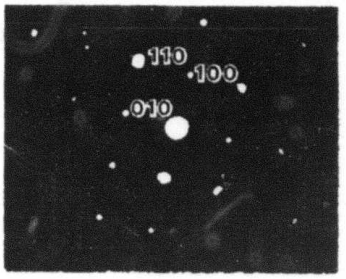

Figure 8: Selected area diffraction (SAD) pattern of a columnar grain.

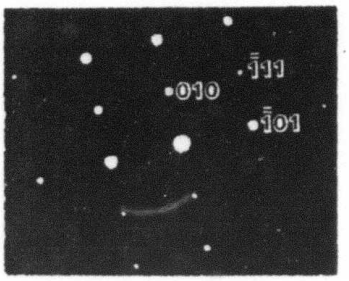

Figure 9: Diffraction pattern taken from a columnar grain and its surrounding eutectic.

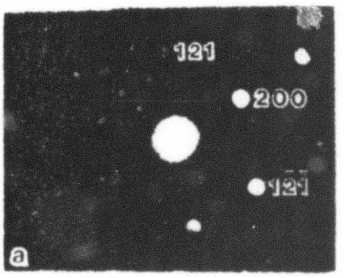

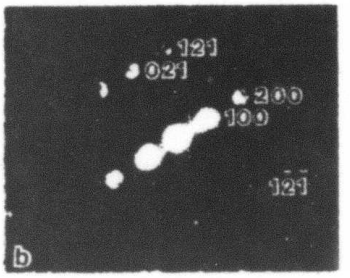

Figure 10: (a) Microdiffraction from rod in eutectic.
(b) Microdiffraction of matrix in eutectic.

consequence of the relatively low tricritical temperature. This fact again is formally similar to the T_o curve for Ag-Cu.

This diagram leads to two important conclusions which are consistent with the experimental results. First, the T_o curve for β-NiAl phase at the eutectic composition occurs at a higher temperature than the T_o curve for the α-Cr phase. Second, if the β-NiAl phase was formed with the eutectic composition directly from the melt, it would undergo subsequent solid state spinodal decomposition into ordered and disordered phases. This type of spinodal has been termed a conditional spinodal [7]. Typical decomposition structures of FeAl by conditional spinodal show coarse antiphase domains of the FeAl along with a fine scale compositional separation into disordered Fe and ordered phase.

The structure of the columnar grains in the present work is identical to the above mentioned structure. The grains contain coarse antiphase domains and fine spinodal structure. This strongly suggests that the columnar grains solidified from the melt as supersaturated β-NiAl rather than supersaturated α-Cr. No antiphase domain boundaries would be visible, if the supersaturated Cr phase had solidified from the melt. The solidification of the ordered phase directly from the melt is also suggested by the fact that at the eutectic composition T_o for the ordered phase is higher than for the disordered phase. Hence, at the eutectic composition partitionless solidification of the β-NiAl phase can occur with less undercooling than that required for the partitionless solidification of the Cr phase.

Eutectic Structure

The solidification of the ribbon is envisioned in two steps. First, the formation of the columnar grains of supersaturated β-NiAl by partitionless solidification followed by the formation of a fine rod eutectic structure in the regions between the columnar grains by near equilibrium solidification. This eutectic solidification would presumably result from the reduction in growth rate caused from the evolution of latent heat during growth of columnar grains. The nucleation of the BCC

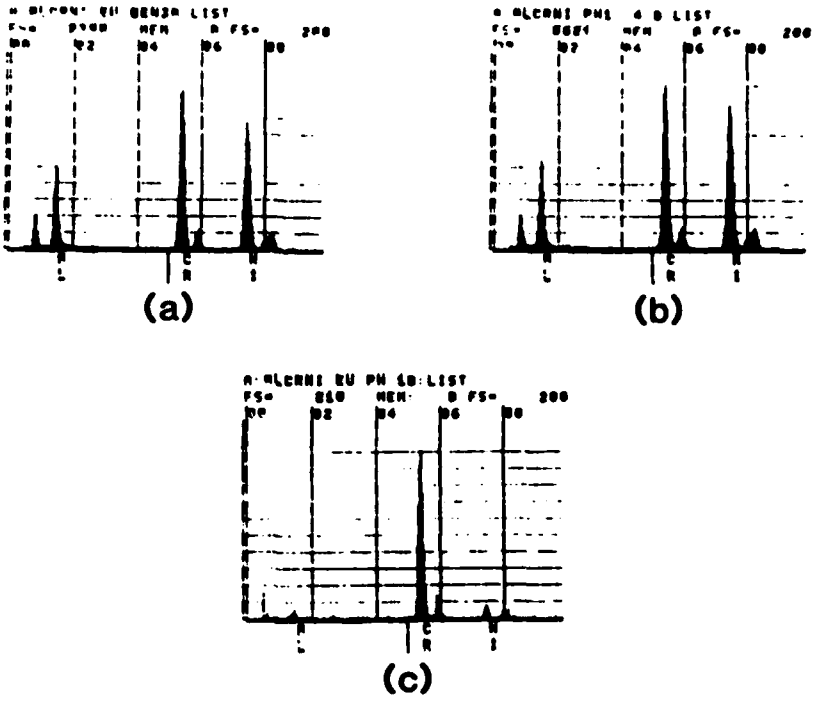

Figure 11: (a) General composition of the ribbon (used as standard). Composition of a columnar grain (b) and of a Cr rod in the eutectic (c).

phase from the CsCl phase seems to be difficult and is demonstrated by the fact that in most cases the eutectic originating from one columnar grain impinges directly upon an adjacent columnar grain. Only rarely do eutectics originating from adjacent grains meet. Once the eutectic has nucleated it rapidly consumes the liquid that remains between the two columns.

The eutectic solidification apparently occurs with near equilibrium compositions for the two solid phases. Although a wide variety of eutectic spacings are seen ranging from 60 nm down to 12 nm the minimum spacings are of particular interest. As described by Boettinger [9] the temperature dependence of the liquid diffusion coefficient leads to a predicted maximum solidification rate for eutectics typically around 10 cm/s. In Ag-Cu eutectic alloys the maximum observed growth rate is 2.5 cm/s with a eutectic spacing of about 20 nm [10]. Hence, the present observation of 12 nm spacing is very interesting. Cline and Walter [2] have measured the rod spacing, λ, as a function of solidification velocity, v, up to 0.021 cm/s. They found these parameters to be related by $\lambda^2 v = 7 \times 10^{-12} cm^3/s$, deduced from their graph. The value of the $\lambda^2 v$ constant for NiAl-Cr is smaller than for Ag-Cu (1.4×10^{-11} cm^3/s) and for most other eutectics [11], presumably because of the low interface energy between β-NiAl and α-Cr phases, that can be attributed to the strong orientation relation and similarity of lattice parameters of the two phases in the eutectic. An experimental determination of the maximum growth rate of the NiAl-Cr eutectic structure will be performed in the future, using electron beam melting experiments.

Acknowledgments

Thanks are due to Dr. Frank Lemkey for pointing out to WJB the similarity of phases in this alloy system and to Dr. John W. Cahn for interpretation of ordered structures. The authors acknowledge the support of DARPA.

References

[1] J. L. Walter, H. E. Cline and E. F. Koch, Trans. TMS-AIME, 245 (1969) 2073.

[2] J. L. Walter and H. E. Cline, Met. Trans., 1 (1970) 1221.

[3] H. E. Cline and J. L. Walter, Met. Trans., 1 (1970) 2907.

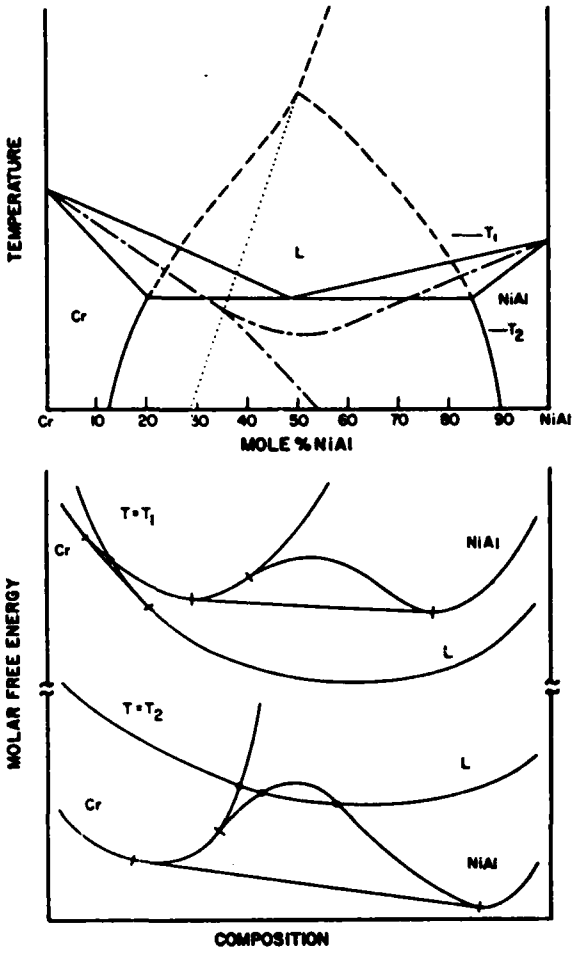

Figure 12: (a) NiAl-Cr phase diagram (solid lines), metastable extension of solvus curves (dashed) to tricritical point and T_0 curves for α-Cr and β-NiAl. (b) Schematic free energy vs composition curves for NiAl-Cr system.

[4] J. L. Walter and H. E. Cline, Met. Trans., 4 (1973) 33.

[5] I. I. Kornilov and R. C. Mintz, Dokl. Akad. Nauk USSR, 94 (1954) 1085.

[6] D. Shechtman, T. Z. Kattamis, F. S. Biancaniello and W. J. Boettinger, to be published, J. Mater. Sci.

[7] S. M. Allen and J. W. Cahn, Acta Met., 24 (1976) 425.

[8] L. D. Landau and E. M. Lifshitz, Statistical Physics, Pergamon Press, London, 1958, p. 434.

[9] W. J. Boettinger, Rapidly Solidified Amorphous and Crystalline Alloys, B. H. Kear, B. C. Giessen and M. Cohen, ed., Elsevier Publishing Company, 1982, p. 15.

[10] W. J. Boettinger, R. Schaefer, F. Biancaniello and D. Shechtman, these Proceedings.

[11] W. Kurz and D. J. Fisher, International Metals Reviews, Nos. 5 and 6 (1979) 177.